Advanced biochar-based materials for specific antibiotics removal from hospital wastewater via adsorption and oxidative degradation

Haotian Xue, Lijuan Deng, Dejun Kang, Ying Zhao, Xinbo Zhang, Ying Liu, Hanyang Chen, Huu Hao Ngo, Wenshan Guo

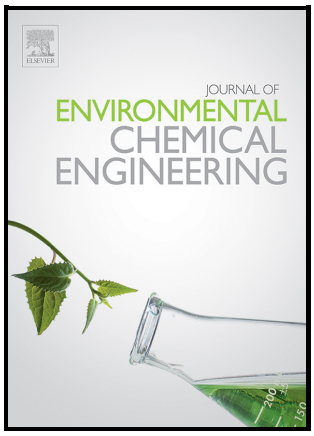

PII: S2213-3437(24)02406-0

DOI: https://doi.org/10.1016/j.jece.2024.114275

Reference: JECE114275

To appear in: *Journal of Environmental Chemical Engineering*

Received date: 21 May 2024
Revised date: 3 September 2024
Accepted date: 26 September 2024

Please cite this article as: Haotian Xue, Lijuan Deng, Dejun Kang, Ying Zhao, Xinbo Zhang, Ying Liu, Hanyang Chen, Huu Hao Ngo and Wenshan Guo, Advanced biochar-based materials for specific antibiotics removal from hospital wastewater via adsorption and oxidative degradation, *Journal of Environmental Chemical Engineering,* (2024) doi:https://doi.org/10.1016/j.jece.2024.114275

Advanced biochar-based materials for specific antibiotics removal from hospital wastewater via adsorption and oxidative degradation

Haotian Xue[a], Lijuan Deng[b,*], Dejun Kang[c], Ying Zhao[a], Xinbo Zhang[d], Ying Liu[d], Hanyang Chen[c], Huu Hao Ngo[b], Wenshan Guo[b,*]

[a] State Key Laboratory of Environmental Criteria and Risk Assessment, Chinese Research Academy of Environmental Sciences, Beijing100012, China

[b] Centre for Technology in Water and Wastewater, School of Civil and Environmental Engineering, University of Technology Sydney, Sydney, NSW 2007, Australia

[c] College of Civil Engineering of Fuzhou University, Fuzhou University, Fuzhou 350108, China

[d] Tianjin Key Laboratory of Aquatic Science and Technology, Tianjin Chengjian University, Jinjing Road 26, Tianjin 300384, China

* Corresponding author: Lijuan Deng, email: lijuan19850317@gmail.com; Wenshan Guo, email: wguo@uts.edu.au

Abstract

Antibiotics in hospital wastewater has become a critical issue due to their potential risks to human health and ecosystems. Biochar as a cost-effective and environmental-friendly carbon material has been employed for removing antibiotics. This article gives a holistic view of the properties of advanced biochar-based materials and clarifies mechanisms on removal of specific antibiotics from hospital wastewater. The increased pyrolysis temperature prepares the modified biochar with higher porosity and larger specific surface for enhancing adsorption. The metal-modified biochar possesses abundant functional groups, limits the leaching of metal ions, and increases the conductivity for improving activation of advanced oxidation process (AOP). Adsorption is significantly affected by the pyrolysis temperature,

solution pH, and properties of modified biochar and antibiotics. The metal-modified biochar-assisted AOP can effectively degrade the pollutants via generating more reactive oxygen species. Weak acidic and/or weak alkaline condition promotes the degradation process in persulfate and peroxymonosulfate systems or during electrochemical oxidation process. Antibiotics removal at a wide pH range (3-11) can be achieved using Fenton-like and photo-Fenton systems with the presence of metal-modified biochar. Future research should focus on development of novel biochar with high reusability and great capability in removing a broad range of specific antibiotics.

Keywords:

Antibiotics; Metal-modified biochar; Adsorption; Degradation; Advanced oxidation process; Mechanism

Abbreviations of antibiotics

AMX, Amoxicillin; **AMP**, Ampicillin; **AZM**, Azithromycin; **CA**, Clavulanic acid; **CAZ**, Ceftazidime; **CED**, Cefradine; **CEP**, Cefepime; **CEZ**, Cefazolin; **CFM,** Cefixime; **CFX**, Cefoxitin; **CHL**, Chloramphenicol; **CIP**, Ciprofloxacin; **CL**, Colistin; **CLA**, Clarithromycin; **CLDM**, Clindamycin; **CLZ**, Clozapine; **CLX**, Cloxacillin; **CPD,** Cefpodoxime; **CRO,** Ceftriaxone; **CTC**, Chlortetracycline; **CTX**, Cefotaxime; **CXM**, Cefuroxime; **DCC**, demeclocycline; **DH**, Doxycycline hyclate; **DOX**, Doxycycline; **DZM,** dimetridazole; **ENR**, Enrofloxacin; **ENX**, Enoxacin; **ERY**, Erythromycin; **GEN**, Gentamicin; **IPM**, Imipenem; **LCM**, Lincomycin; **LEV**, Levofloxacin; **LEX**, Cefalexin; **LOM**, Lomefloxacin; **LRZ**, Lorazepam; **MEM**, Meropenem; **MET**, Metronidazole; **NA**, Nalidixic acid; **NOR**, Norfloxacin; **OFL**, Ofloxacin; **OTC**, Oxytetracycline; **OXZ**, Oxazepam; **PEN**, Penicillin; **PIP**, Piperacillin; **ROX**, Roxithromycin; **SDX**, Sulfadoxine; **SDZ**, Sulfadiazine; **SFZ**, Sulfamethizole; **SMP**, Sulfamethoxypyridazine; **SMR**, Sulfamerazine; **SMX**,

Sulfamethoxazole; **SMZ**, Sulfamethazine; **SPC**, Spiramycin; **SPY**, Sulfapyridine; **TAZ**, Tazobactam; **TC**, Tetracycline; **TMP**, Trimethoprim; **TNZ**, Tinidazole; **TYL**, Tylosin; **VAM**, Vancomycin

Abbreviations of biochar-based products

AC, prepared by impregnating primary paper mill sludge with potassium hydroxide at ratio of 1:1 (w/w), followed by pyrolyzing at 800 ºC for 1.5 h;

AFAC, prepared by immersing *Azolla Filiculoides* (water fern) powder into $ZnCl_2$ solution, followed by pyrolyzing at 350 ºC for 2 h and 600 ºC for 4 h;

AMBC, prepared by placing rice husk biomass at a pyrolysis temperature of 500 ºC (pristine biochar), followed by mixing with montmorillonite solution, and keeping at 500 ºC with N_2, then switching to CO_2 gas for activation of the biochar;

BC700, prepared by pyrolyzing spiramycin fermentation residue (SFR) powder at 700 ºC for 2 h;

PCB-900 ºC, prepared by pyrolyzing pine cones at 900 ºC;

BDB, prepared by pyrolyzing at 550 ºC for 1.5 h to obtain biosolids-derived biochar;

SCGDB, prepared by obtained by pyrolyzing at 550 ºC for 1.5 h to obtain spent coffee grounds-derived biochar;

$CoFe_2O_4$/NiO@N-PAC, prepared by hydrothermal co-carbonisation of N-rich *Spirulina platensis* (Sp) microalga and glucose, followed by chemically activating with KOH at 700 ºC to obtain N-PAC, and finally mixing $CoFe_2O_4$/NiO nanoparticles with N-PAC;

$CoFe_2O_4$@CMC/HZSM-5, prepared by dissolving iron chloride ($FeCl_3 \cdot 6H_2O$) and cobalt chloride ($CoCl_2 \cdot 6H_2O$) in distilled water, followed by adding carboxymethylcellulose (CMC) and H form or protonic type of Zeolite Socony Mobil-5 (HZSM-5 zeolite), then adjusting pH to 11, and finally being irradiated by microwave and dried in the oven (100 ºC);

CS-AC, HS-AC, and RH-AC, prepared by mixing corn stalk (CS), hazelnut shell (HS), and rice husk (RH) with potassium hydroxide (w:w, 1:1), respectively, followed by applying the flash heating method in a reactor system with a moving furnace at 950 ºC;

Fe-Ce@N-BC, prepared by sonicating banyan branch powder in aqueous solution containing urea with mass ratios of urea to banyan branch powder at 2:1, followed by adding into mixture of $Ce(NO_3)_2 \cdot 6H_2O$ and $Fe(NO_3)_3 \cdot 9H_2O$, and subsequently pyrolyzing at 800 ºC;

Fe/N-biochar, prepared by dissolving dicyandiamide, $FeCl_3 \cdot 6H_2O$ (mass ratio of 0.5) and sawdust, followed by pyrolyzing at 800 ºC;

Fe_1:Co_2-bwc/LBE, prepared by 1) pre-treating bagassewaste carbon (bwc) with H_2SO_4 solution; 2) soaking into bimetal-oxide (Fe and Zn) solution with Fe & Co molar ratio of 1:2; 3) calcinating at 350 ºC, dipping into 0.1 M metal oxide and 0.1 M Hexamethylene tetramine (HMTA) solution inside Teflon lined hydrothermal reactor, putting into the oven at 90 ºC for 3 h, and separating and drying at 300 ºC; 4) mixing solid powered materials in preheated binder solution of Polyvinylidene fluoride (PVDF) and N-methylpyrrolidone (NMP); 5) coating the obtained products on a commercial modified lead oxide battery electrode (LBE) and drying at 140 ºC overnight;

FMPC, prepared by mixing $FeCl_3$ and $FeSO_4$ solutions with pine cones;

GPH, prepared by hydrothermal carbonisation of grapefruit peel at 180 ºC for 12 h, subsequently immersing into alcohol and deionised water for 12 h, and finally drying at -60 ºC for 50 h to obtain brown product, namely grapefruit peel aerogel;

MGPH, prepared by using 0.5 g of GPH and 0.5 g of dopamine in Tris solution, followed by stirring for 5 h at 70 ºC;

KMBC, prepared by adding pretreated wood chips into aqueous solution containing Fe^{2+} and K^+ at the mass ratio of wood chips, iron and potassium content was 5:1:1, followed by pyrolyzing at 600 ºC to obtain potassium-doped magnetic biochar;

MAGB, prepared by soaking garlic skin fine powder into $FeCl_3$ solution, followed by mixing with $ZnCl_2$ and pyrolyzing at 800 ºC;

MBC, prepared by adding pretreated *Eichhornia crassipes* (water hyacinth) into Fe^{2+} solution to obtain the Fe(II)-laden water hyacinth, followed by pyrolyzing at 400 ºC;

MFe_2O_4@BC (M = Co, Cu and Mn), prepared by dissolving $Co(NO_3)_2 \cdot 6H_2O$, $Cu(NO_3)_2 \cdot 3H_2O$ and $Mn(NO_3)_2 \cdot 4H_2O$ into absolute ethanol with $Fe(NO_3)_3 \cdot 9H_2O$ at the ratio of 1:2, respectively, subsequently adding nitric acid-pretreated coconut shell-derived biochar, and finally calcinating at 400 ºC for 3 h;

MnFe-LDO-biochar, prepared by adding palm seeds into mixed solutions of $FeCl_3 \cdot 6H_2O$ and $MnCl_2 \cdot 4H_2O$, followed by calcinating at 600 ºC (LOD, layered double oxides);

MMBC, prepared by soaking pine sawdust into manganese sulphate, followed by pyrolyzing at 600 ºC;

MPBC, prepared by soaking polar wood into KOH solution, followed by pyrolyzing at 500 ºC for 2 h to obtain polar wood biochar (PBC), subsequently adding $NH_4(FeSO_4)_2 \cdot 12H_2O$, $(NH_4)_2Fe(SO_4)_2 \cdot 6H_2O$ and PBC to distilled water, then adding $NH_3 \cdot 2H_2O$ into aforementioned mixture;

Ni-MMR, prepared by modifying the microbial residue (the *Pichia pastoris* yeast residue) with PEI solution and 25% glutaraldehyde to adsorb Ni(II) in the adsorption system with 100 mg/L Ni(II) at pH 5;

Ni-MMC, prepared by mixing Ni-MMR and potassium hydroxide, followed by pyrolyzing Ni-MMR at 700 ºC;

NMBC, prepared by mixing pine sawdust and ferrous sulphate for 2 h, followed by pyrolyzing at 600 ºC for 2 h, and finally adding urea;

NZVI/Cu^0/BC-3, prepared by pre-treating the Banyan branch with KOH and HCl solution, followed by mixing $Fe(NO_3)_3 \cdot 9H_2O$ and $Cu(NO_3)_2 \cdot 3H_2O$ with the pre-treated Banyan branch

at metal salt to Banyan branch power mass ratio of 3:1, and finally pyrolyzing at 800 ºC in the nitrogen condition for 2 h;

PCB-900 ºC, prepared by pyrolyzing pine cones at 900 ºC;

P200 and P400, prepared by pyrolyzing peanut shell powder at 200 ºC and 400 ºC, respectively;

PBC-400CuFe, prepared by soaking coconut shell in nitric acid solution to obtain the pretreated biochar (PBC), followed by impregnating using Fe(III)-Cu(II)-ethanol solution with a Cu/Fe molar ratio of 1:2, and subsequently calcinating at 400 ºC;

PBFG4, provided by ChemViron Carbon as commercially available activated carbon;

PCoF, prepared by adding the mixed solution of $Co(NO_3)_2 \cdot 6H_2O$ and $Fe(NO_3)_3 \cdot 9H_2O$ at the ratio of 1:2 into pretreated coconut shell-derived biochar, followed by calcinating at 400 ºC for 3 h;

PJAC, prepared by carbonising the dried chips of prosopis juliflora branches with 1:1 w/w H_2SO_4, followed by drying overnight at 100 ºC and completely carbonising at 500 ºC;

PT500, prepared by pyrolyzing sugarcane bagasse at 500 ºC for 2 h;

PTBC, prepared by pyrolyzing palm tree bark biomass at 500 °C;

PZBC800, prepared by soaking pharmaceutical sludge in $ZnCl_2$ solution, followed by pyrolyzing at 800 ºC;

RM-NPs, prepared by mixing $FeCl_3 \cdot 6H_2O$, $FeCl_2 \cdot 4H_2O$ and red mud (RM) in deionised water and stirring under nitrogen gas at 80 ºC for 1 h, followed by adding NH_4OH and stirring for 1 h, to obtain magnetite (Fe_3O_4) nanoparticles (NPs) combined with RM;

SMBC600, prepared by immersing sugarcane bagasse powder in diluted steel pickling waste liquor (total iron ratio = 12 g/L), followed by pyrolyzing at 600 ºC;

SMBC300, SMBC400 and SMBC500, prepared by pyrolyzing sugarcane bagasse and steel pickling waste liquor at temperatures of 300 °C, 400 °C, and 500 °C, respectively;

ZnO/PiC0.1, prepared by soaking o.1 g of pine carbon in NaOH solution to obtain pine alkaline hydrolysate (PiC0.1), followed by adding PiC0.1 to $ZnCl_2$ solution, and subsequently heating at 180 ºC for 12 h

1. Introduction

High quantities of wastewaters are generated from global hospitals with an average of around 750 L/bed·day, which are far more than the wastewaters produced by conventional households (~ 100 L/capita·day) (Suarez et al., 2009; Top et al., 2020). Hospital wastewaters are generally divided into domestic discharges and the effluents specific to hospitals which are generated by care, diagnosis, analysis, equipment disinfection and research activities. The effluents contain a great variety of toxic substances, such as pharmaceuticals, detergents, radioelements, pathogenic microorganisms, contagious faeces, etc. (Boillot et al., 2008; Top et al., 2020). A large number of pharmaceuticals from hospital wastewaters enters the aquatic environment due to the limited removal by onsite treatment systems or centralised plants, and direct release from untreated discharges into receiving waters (Han et al., 2022; Tahiri et al., 2023; Zhou et al., 2023).

Among different types of pharmaceuticals, antibiotics used in human medicine to prevent and treat infectious diseases have attracted great attentions as the presence of antibiotics in the environment not only exerts ecotoxic effects on organisms, but also prompts the development of antibiotic-resistant bacteria (ARB) and antibiotic resistance genes (ARGs) and their spread, giving rise to adverse effects on human health and ecosystems (Ngigi et al., 2020). Common antibiotics frequently detected from hospital wastewater at high levels in different regions of the world (e.g., India, Iran, United States, Tunisia, Singapore, Qatar, Romania, Colombia, etc.) are mainly classified into ten groups, namely sulfonamides (e.g., SMX (up to 96.02 μg/L), etc.), reductase inhibitor (e.g., TMP (up to 90.00 μg/L), etc.),

quinolones (e.g., CIP (up to 1830.00 μg/L), NOR (up to 561.00 μg/L), OFL (up to 5350.80 μg/L), etc.), tetracyclines (e.g., TC (up to 29.10 μg/L), OTC (30.05 μg/L), CTC (28.64 μg/L), etc.), macrolides (e.g., ERY (up to 83.00 μg/L), CLA (up to 159.73 μg/L), AZM (up to 400.00 μg/L, etc.), SPC (up to 45.30 μg/L), etc.), glycopeptide (e.g., VAM (up to 43.74 μg/L), etc.), cephalosporin/β-lactams (e.g., CEP (up to 540.39 μg/L), CPD (4080.00 μg/L), CAZ (up to 31.21 μg/L), CRO (up to 59.50 μg/L), etc.), penicillins/β-lactams (e.g., AMX (up to 4000.00 μg/L), AMP (up to 53.00 μg/L), etc.), lincosamides (e.g., CLDM (up to 25.40 μg/L), etc.), nitroimidazole (e.g., MET (up to 258.30 μg/L), etc.) (Ajala et al. et al., 2022; Aydin et al., 2018; Cai et al., 2022a; Fatimazahra et al., 2023; Lien et al., 2016; Moratalla et al., 2022; Omuferen et al., 2022; Pariente et al., 2022; Szekeres et al., 2017; Segura et al., 2021; Ulvi et al., 2022; Yao et al., 2021).

As a cost-effective and environmental-benign carbon-rich product derived from biomasses or biowastes, biochar possesses highly porous structure, large specific surface area, abundant functional groups and stable chemical properties. Therefore, biochar has been increasingly used for adsorption and removal of diverse pollutants (Herrera et al., 2022; Liu et al., 2020; Xu et al., 2022). The applications of biochar in the removal of the common antibiotics (e.g., SMX, SDZ, TMP, CIP, NOR, OFL, TC, ERY, AMX, etc.) from waters and wastewaters have become a major focus of recent studies, as demonstrated in latest review articles, such as biochar and modified biochar for the adsorption of the common antibiotics (Anuar et al., 2023; Ding et al., 2023; Du et al., 2023; Katiyar et al., 2022; Krasucka et al., 2021; Liu et al., 2020; Ouyang et al., 2020; Mahari et al., 2022), biochar-based nanohybrids or Fe-based bimetallic persulfate activation catalysts for degradation of the antibiotics via activation of peroxymonosulfate or peroxydisulfate (Liu et al., 2023; Zhang et al., 2024), straw-derived biochar and the modified biochar for adsorption and degradation of the antibiotics (Zhang et al., 2023a), etc. However, it still lacks the systematic and detailed

discussion on different types of modified biochar for the removal of specific antibiotics which are used to treat varying infections or anxiety disorders, and less reported for hospital wastewater treatment (e.g., CLA, AZM, SPC, DZM, CLDM, MET, ENX, OXZ, LRZ, etc.). Therefore, this paper aims to provide a comprehensive review about applications of biochar-based products in the removal of the specific antibiotics using various treatment methods. More specifically, it deeply discusses the properties of different types of biochar-based products (including modified biochar prepared at high pyrolysis temperature and metal-modified biochar) responsible for enhancing removal of the specific antibiotics. It also elucidates the removal mechanisms with respect to the adsorption and degradation in the advanced oxidation process, respectively. The suggestions are finally given on the methods for improving the properties of the biochar-based products and on the future research directions for extending their application.

2. Applications of modified biochar for enhancing removal processes

2.1. Modified biochar for enhancing adsorption process

Some methods (e.g., pyrolysis, flash heating, metal-based modification) have been developed to improve properties (e.g., aromaticity, pore volume, specific surface area, functional groups, etc.) of pristine biochar favourable for adsorption of antibiotics. Latest studies on modified biochar prepared from different methods and their applications in removal of specific antibiotics have been listed in Table 1. As to the pyrolysis method, the increased pyrolysis temperature reduces the contents of oxygen (O) and hydrogen (H), while elevating carbon (C) content of biochar. The declined H/C and increased C/N at higher pyrolysis temperature demonstrate the increase in the aromaticity and hydrophobicity of biochar. Additionally, higher pyrolysis temperature also increases specific surface area (Table 1; e.g., 597.97 m^2/g of PCB-900 ºC vs 64.77 m^2/g of PCB-500 ºC and 353.97 m^2/g of PCB-

700 ºC) and micropore volume (e.g., 0.24 cm^3/g of PCB-900 ºC vs 0.026 cm^3/g of PCB-500 ºC and 0.156 cm^3/g of PCB-700 ºC) owing to the formation of the vascular bundle structure of the biochar by the release of volatile components (Chebbi et al., 2023; Herrera et al., 2022; Sun et al., 2018; Wu et al., 2022). The obtained biochar (i.e., PJAC, PTBC) possesses abundant functional groups, such as -OH, C-O, C=O, C=C, C-N, N-H, and C-C, for adsorption (Azeez et al., 2024; Manjunath and Kumar, 2018). Carbon aerogel as a kind of porous materials prepared by pyrolyzing organic aerogels under inert gas condition has also been used for adsorption of targeted pollutants. The modified biochar aerogel (i.e., MGPH) had high specific surface area due to formation of an open three-dimensional network structure, as well as exhibited porous structure, high expansibility, low density, and abundant functional groups, such as -OH, $-CH_2$, N-H, Ph-OH, and C=C (Bai et al., 2023).

Table 1.

However, the extremely high pyrolysis temperature may either deteriorate the structure of biochar and cause pore blocking or destroy pore structure as it can deteriorate pore walls and change small pores into larger ones (Hu et al., 2024; Wu et al., 2022). Additionally, this heating method requires thermal gradient, which not only limits the effective release of gas products and induces carbon deposition, but also adversely affects the quality of the obtained biochar, giving rise to formation of inhomogeneous microporous networks. The slow heating rate during pyrolysis process increases operational cost and energy consumption (Yurtay and Kılıç, 2023). Hence, Yurtay and Kılıç (2023) employed the flash heating method to prepare biochar, in which the furnace with the fixed carbonisation temperature of 950 ºC moved through the biomass in a quartz tube for carbonisation/activation process. The furnace was subsequently moved back to its original place, and finally the carbonised samples were taken out. The whole process lasted for about 15 min. The obtained biochar displayed

homogeneous pore structure, as well as high specific surface area (up to ~ 2305 m^2/g), large total pore volume (up to ~ 2.00 cm^3/g), high microporosity (micropore volume, up to 0.9500 cm^3/g) and great external surface area (up to ~ 984 m^2/g) (Table 1).

In recent years, metal-modified biochar has been frequently synthesised for adsorption of specific antibiotics. Hu et al. (2024) modified the microbial residue (the *Pichia pastoris* yeast residue) by employing polyethyleneimine (PEI), which enabled the modified residue with increased roughness and metal binding sites for adsorption of Ni(II) to obtain Ni-MMR. Then Ni-MMR was pyrolyzed to generate the metal-modified biochar (Ni-MMC) exhibiting faster adsorption of MET (equilibration time, 15 min) compared with MMC (> 15 min). More studies focus on synthesis of Fe-modified biochar using iron salts, enabling the biochar to be easily separated from aqueous solutions by an external magnetic field. Thus, this type of Fe-modified biochar can be also named as magnetic biochar, which not only allows effective recycling process of the biochar, but also enhances the adsorption of the targeted pollutants on the biochar for the effective removal of the pollutants. Some studies mixed Fe^{2+} and Fe^{3+} ions-containing solution (e.g., $FeCl_3 \cdot 6H_2O$ + $FeCl_2 \cdot 4H_2O$, $FeCl_3$ + $FeSO_4$, $NH_4Fe(SO_4)_2 \cdot 12H_2O$ + $(NH_4)_2(FeSO_4)_2 \cdot 6H_2O$) with biowaste (i.e., red mud, pine cones, poplar wood powder) to obtain Fe-modified biochar with abundant functional groups, such as –OH, C≡C, C=C, C=O, C–O, C-O-C, and O-C=O (Aydın et al., 2021; Aziz et al., 2024; Zhang et al., 2023b). The obtained biochar (FMPC and RM-NPs) prepared with iron ions-containing solution ($FeCl_3 \cdot 6H_2O$ + $FeCl_2 \cdot 4H_2O$, or $FeCl_3$ + $FeSO_4$) presented specific surface morphology (e.g., iron particles dispersed into the carbon matrix, cylindrical cavities and cracks, high roughness), which increased specific surface area favourable for the adsorption process (Aydın et al., 2021; Aziz et al., 2024). However, the specific surface areas and pore volume of MPBC prepared using $NH_4Fe(SO_4)_2 \cdot 12H_2O$ and $(NH_4)_2(FeSO_4)_2 \cdot 6H_2O$ were lower (122.12 m^2/g and 0.38 cm^3/g, respectively) than those of the pristine biochar (PBC,

165.18 m^2/g and 0.46 cm^3/g, respectively) as magnetic particles (e.g., Fe_3O_4 nano-particles) deposited on the surface of MPBC blocked its pores (Feng et al., 2022; Zhang et al., 2023b). Hence, the precursors of iron ions-containing solution with chloride ions (e.g., $FeCl_3$, $FeCl_2$) rather than those with sulphate ions (e.g., $NH_4Fe(SO_4)_2$, $(NH_4)_2(FeSO_4)_2$) may be more suitable for synthesise of the metal-modified biochar with high specific surface area and pore volume for enhancing adsorption process.

To increase specific surface area and pore volume of the biochar, a simultaneous activation and magnetisation method has been developed and employed. More specifically, both $ZnCl_2$ and $FeCl_3$ reagents were introduced simultaneously into the framework of the agricultural waste (e.g., garlic skin) to obtain MAGB. During the preparation process, $ZnCl_2$ was adopted as the activating agent to enlarge the specific surface area of biochar and stimulate pore formation via a series of reactions ($ZnCl_2 + H_2O \rightarrow H[ZnCl_2(OH)]$, $H[ZnCl_2(OH)] \rightarrow ZnO + HCl\uparrow$, $2ZnO + C \rightarrow 2Zn + CO_2\uparrow$, $ZnO + C \rightarrow Zn + CO\uparrow$), while $FeCl_3$ was used to provide magnetic features. The biochar obtained (MAGB) exhibited higher pore volume and specific surface area (0.51 cm^3/g and 1008.97 cm^2/g, respectively) than the unmodified biochar (GB, 0.42 cm^3/g and 599.95 m^2/g, respectively), as well as possessed abundant oxygen-rich functional groups (metal-O, C=O and C-OH bonds) (Feng et al., 2022). Another kind of the novel biochar is the modified biochar derived from N-rich biomass (N-rich *Spirulina platensis* (Sp) microalga) and $CoFe_2O_4$/NiO nanoparticles (e.g., $CoFe_2O_4$/NiO@*N*-PAC), which contains the pyrrolic-N and graphitic-N on its surface responsible for enhanced adsorption process (Ameen et al., 2023). To improve the properties of metal-modified biochar, the H form or protonic type of Zeolite Socony Mobil-5 (ZSM-5) was applied due to its high porosity, ion exchange ability, thermal stability, and mechanical strength. $CoFe_2O_4$@CMC/HZSM-5 derived from carboxymethylcellulose as a mesoporous

material exhibited abundant functional groups, including -OH, -COOH and C-O, contributing to high adsorption capability (Nasiri et al., 2022).

2.2. Modified biochar for enhancing activation of advanced oxidation process (AOP)

During advanced oxidation process (AOP), metal-modified biochar can activate oxidants (e.g., persulfate (PS), peroxymonosulfate (PMS), hydrogen peroxide (H_2O_2), etc.) in aqueous solution to generate reactive oxygen species (ROS) for degrading pollutants. Nevertheless, the Fe-modified biochar in the AOP suffers from low oxidation efficiencies of organic pollutants. Fe(II) plays a key role in activating PS (Luo et al., 2022 and 2023a). Hence, some modification methods have been developed to increase Fe(II) content in the metal-modified biochar: 1) introducing transitional metal (e.g., magnesium (Mn)), which enabled the loading of metal oxides ($MnFe_2O_4$) on the surface of the metal-modified biochar (MMBC), enlarged the specific surface area, elevated Fe(II) content in the biochar, and increased the content of reducing functional groups (O=C, C=C) as activation sites for activating PS (Luo et al., 2023a); 2) doping non-transitional metal without leaching risk (e.g., potassium) to obtain the metal-modified biochar (KMBC), which encouraged the production of carbon monoxide (CO) and hydrogen (H_2) during the pyrolysis process. Both CO and H_2 facilitated the conversion of Fe(III) to Fe(II). Additionally, the presence of potassium also enabled the uniform distribution of iron species on the metal-modified biochar for improving its activation performance (Luo et al., 2022); 3) doping exogeneous nitrogen (i.e., urea) to increase nitrogen content in the metal-modified biochar (NMBC), which promoted the formation of defective carbon and graphitised structure, and improved electrochemical conductivity and the electron transfer speed of the biochar. Additionally, it also increased the content of the reducing functional groups (O=C, C≡N, C=C) as activation sites. More importantly, Fe(II) content also increased in the biochar as N stimulated strong electron

donors to Fe atom by the coordination bound, thereby elevating the electron density on the Fe atom (Fig. 1(a)). These properties obtained encouraged the activation of PS (Luo et al., 2023b).

Loading metal species into N-doped biochar (e.g., Fe-N-biochar) could increase active reaction sites for activating PMS. However, the biochar obtained is presented as bulky aggregates with disarranged size and morphology. Additionally, metal ions may also be leached from the biochar, resulting in declined activation performance and secondary pollution. As a result, Fe-based oxides has been taken into account due to their stability. Notably, aqueous mixture containing Ce(IV) (i.e., $Ce(NO_3)_2 \cdot 6H_2O$) and Fe(III) (i.e., $Fe(NO_3)_3 \cdot 9H_2O$) was used for preparation of Fe-Ce@N-BC, which inhibited the leaching of Fe ions via the conversion cycle of Ce(III) and Ce(IV) and strong interaction of Ce(III)/Ce(IV) with Fe oxides during the PMS activation process (Xiao et al., 2022). Compared to metal ions (e.g., Fe^{2+}), zero-valent metals (e.g., Fe^0 nanoparticles (NZVI)) more effectively activate PMS due to its low reduction potentials (e.g., $E^0(Fe^{2+}/Fe^0)$ = -0.44 V). However, the pristine NZVI is prone to corrosion and aggregation. Thus, zero-valent bimetallic materials have been increasingly explored to enhance electron transfer and degradation of targeted pollutants. Recently, Xu et al. (2024) developed the bimetallic NZVI/Cu^0/BC-3 composite using $Fe(NO_3)_3 \cdot 9H_2O$ and $Cu(NO_3)_2 \cdot 3H_2O$, which possessed more defective sites than pristine biochar for enhancing activation of PMS, and presented a 3D hierarchical flower-like shell/core structure with Fe^0 and Cu^0 species wrapped by carbon nanosheets. The biochar at the outer layer not only limited the release of metal species during the activation process of PMS, but also adsorbed the released metal species for further regeneration of the biochar under N_2 atmosphere. Hence, this structure could completely expose active sites and enable the stability of the biochar.

As a novel kind of H_2O_2 activators, the metal-modified biochar (e.g., MBC) has been used in Fenton-like process to promote the production of ROS (e.g., hydroxyl radicals (·OH)) due to the presence of Fe(II) in the biochar (Yi et al., 2021). However, the activation of H_2O_2 by Fe(II) needs to be operated at acidic pH of 3.0 for generating ·OH. This leads to higher operational cost owing to the requirement of alkaline reagents for adjusting pH of the effluent from Fenton-like process, in order to achieve neutral pH for subsequent biological treatment system. Heterogeneous photo-Fenton combining adsorption, photocatalysis and reactive oxygen species can increase pH in the Fenton-like process to some extent (Cai et al., 2021).

Bimetallic iron-based oxide spinels (magnetic MFe_2O_4, M (transitional metals) = Co, Cu, Mn, Zn) have attracted great attention as the promising photocatalysts in the photo-Fenton process since they possess a relatively narrow bandgap, and excellent visible-light response. To avoid the demerits of MFe_2O_4 (e.g., fast recombination of electron-hole pairs, leaching of transitional metal ions, low specific surface area), current studies have used the biochar as a carrier to prepare magnetic MFe_2O_4@BC via impregnation and calcination method. The pristine biochar was pretreated by nitric acid solution to obtain pretreated biochar, which was mixed with $Fe(NO_3)_3 \cdot 9H_2O$, $M(NO_3)_X \cdot aH_2O$ (e.g., $Co(NO_3)_2 \cdot 6H_2O$, $Cu(NO_3)_2 \cdot 3H_2O$) and ethanol solution for the impregnation, and subsequently calcinated at high temperature (e.g., 400 ºC) (Cai et al., 2021; Cai et al., 2023). This method increases specific surface area and total pore volume of the novel photo-Fenton catalyst by introducing biochar. Moreover, biochar as carbon-rich and electrically conductive material helps to enhance the separation rate of the electron-hole pairs. The couplings between Fe(III)/Fe(II) and M(x-1)/M(x) redox pairs (x = valence state, e.g., M(x-1)/M(x) = Co(II)/Co(III), Cu(I)/Cu(II)) over the surface of MFe_2O_4@BC during the photo-Fenton process could minimise the leaching of metal ions, and induce generation of more ·OH. Moreover, the

modified biochar has high stability and recyclability, i.e., almost 90% removal of MET after five degradation cycles (Azalok et al., 2021; Cai et al., 2021; Cai et al., 2023).

The electrochemical oxidation process has also been explored for the degradation of specific antibiotics. Sharan et al. (2023) prepared Fe_1:Co_2-bwc/LBE through doping bimetal-oxide (Fe and Zn) nanoparticles on bagassewaste carbon (bwc) and further on a commercial modified lead oxide battery electrode (LBE). The introduction of bimetal-oxide particles increased the oxygen evolution potential of the biochar (OEP, 1.44 V vs 1.14 V for Fe and 1.20 V for Zn for the electrode prepared by single metal-oxide), improved the conductivity, provided more surface area for electron mass transfer favourable for redox reaction, and stimulated the generation of more ·OH radicals for MET degradation during electrochemical oxidation process. However, this modified biochar suffered from release of metal ions after three degradation cycles, resulting in a decline in MET removal from 89.8% in the first cycle to 71.8% in the third cycle (Sharan et al., 2023). Therefore, developing novel biochar with high reusability for removal of specific antibiotics is an essential task in the future.

3. Removal pathways

3.1. Adsorption

The adsorption mechanisms are considerably affected by the pyrolysis temperature employed for preparation of biochar and solution pH during the adsorption process. The elevated pyrolysis temperature increases aromatic structure of the biochar (e.g., PCB-900 ºC), which enhances π-π interaction between aromatic rings of biochar and those of MET. At higher pyrolysis temperature, the improved pore structure of the biochar is favourable for pore filling mechanism (Chebbi et al., 2023). Additionally, hydrogen-bonding also involves in the adsorption of MET, DZM and SPC at higher pyrolysis temperature (i.e., 500 ºC, 700

ºC) due to the presence of oxygen-containing functional groups in the modified biochar (e.g., -OH and -COOH in PT500, C-C and O-C=O in BC700) (Gao et al., 2022; Sun et al., 2018).

Another important adsorption mechanism, electrostatic attraction, is affected by solution pH and strongly correlated with pKa of the targeted compounds and point of zero charge (pH_{pzc}) of biochar. Ka is the equilibrium constant of the dissociation reaction of an acid. Ka1 and Ka2 are the constants for the dissociation of first and second protons from polyprotic acid, respectively (Helmenstine, 2019). pKa, pKa1, and pKa2 are the negative base -10 logarithms of the acid dissociation constants of a solution (i.e., $pKa = -\log_{10}Ka$, $pKa1 = -\log_{10}Ka1$, $pKa2 = -\log_{10}Ka2$; pKa1 < pKa2) (Byju's, 2024). pH_{pzc} indicates the pH value at which the surface of biochar presents zero or neutral electrical charge (Ameen et al., 2023).

Generally, the targeted antibiotics are present in the cationic form when pH is below pKa (or pKa1), while the higher pH (> pKa or pKa2) induces the compounds to exist as anionic form (Arif et al., 2023; Chebbi et al., 2023). As to biochar, OH^- ions deprotonate the surface functional groups at lower pH (< pH_{pzc}), leading to generation of positive charges on the surface. At pH higher than pH_{pzc}, the surface functional groups on biochar are deprotonated by H^+ ions to form negative charges on the biochar surface (Ameen et al., 2023; Balarak et al., 2021). pH_{pzc} value is normally less than pKa or pKa2 value. Thus, the maximum adsorption of targeted pollutants on biochar may be realised at pH ranging from pH_{pzc} value to pKa or pKa2 value. For example, the maximum adsorption of AZM (Pka = 8.60-9.50) on biochar (e.g., $CoFe_2O_4$/NiO@*N*-PAC (pH_{pzc} = 6.90), AMBC) occurred at pH at 7.00 (Ameen et al., 2023; Arif et al., 2023). MPBC (pH_{pzc} = 6.45) demonstrated strong electrostatic attraction for ENX (pKa1 = 6.0, pKa2 = 8.5) at pH of 6-7 (Zhang et al., 2023b).

However, the importance of electrostatic attraction may decline with a large difference between pKa1 value and pKa2 value. At pH of 4-11, MET exists in the neutral form based on its properties (pK_{a1} =2.58, pK_{a2} =14.4). Hence, regardless of pH_{pzc} of biochar, pH has a slight

influence on the removal of MET, leading to minor effects of electrostatic interaction on the adsorption process (Chebbi et al., 2023; Feng et al., 2022; Hu et al., 2024). Some studies pointed out that the maximum adsorption of MET by the modified biochar occurred at pH of 6-7.2, which was mainly controlled by hydrogen bonding interactions, π-π interaction, CH/COOH/OH-π interaction, and complexation formation via interaction of MET electron donating groups with the metal ions (withdrawing groups) on the biochar (Azeez et al., 2024; Nasiri et al., 2022). When applying biochar for LRZ removal, π-π interaction rather than electrostatic interaction dominated the adsorption process at pH of 5.5-7.6 due to the non-ionizable form of LRZ (pKa_1 =1.3, pKa_2 = 11.5) (Jaria et al., 2020). It should be noted that other mechanisms also take part in the adsorption when using the modified biochar with unique characteristics. More specifically, at neutral pH, AMBC obtained by coating clay minerals with high ion exchange capability could enable ion exchange between negatively charged silanol groups (≡ Si-OH) of AZM and negatively charged surface of AMBC (Arif et al., 2023). $CoFe_2O_4$/NiO@*N*-PAC could strengthen adsorption ability via Lewis's acid–base interaction between pyrrolic- N of the biochar (the Lewis-base site) and (-OH) Lewis-acid site of AZM (Ameen et al., 2023).

3.2. Metal-modified biochar-assisted AOP

Metal-modified biochar with or without nitrogen doping encourages the generation of $^1O_2$ and ·OH radicals in the PS system for degrading pollutants (i.e., MET). MET was finally converted to acetic acid, N-ethylglycine, formic acid and oxalic acid through three different pathways (Fig. 1; Luo et al., 2022; Luo et al., 2023a and 2023b).

Fig. 1.

Metal-modified biochar/PMS system involves the degradation of MET mainly through activating PMS to generate $SO_4^{-\bullet}$, $O_2^{\bullet-}$, and ·OH radicals for free radical pathway and $^1O_2$ species for non-radical pathway (Fig. 2). Regarding Fe-Ce@N-BC, $SO_4^{-\bullet}$, $O_2^{\bullet-}$, and ·OH radicals were generated through activation of PMS using Ce(III) and Fe(II), and interaction between PMS and free-flowing π-electrons from sp^2 carbons of biochar (pyridinic N in the carbon framework stimulated the transfer of the π-electrons from biochar). Additionally, $O_2^{\bullet-}$ involved in converting Ce(IV) and Fe(III) into Ce(III) and Fe(II) via electron transfer (Xiao et al., 2022; Fig. 2a). As to NZVI/Cu^0/BC-3, both Fe^0 and Cu^0 activated PMS to release $SO_4^{-\bullet}$ and ·OH radicals. Additionally, the generated Fe(II) and Cu(I) also stimulated the production of $SO_4^{-\bullet}$ by reacting with HSO_5^-. The redox cycle and one-electron reaction induced the formation of Fe(II) favourable for activating PMS (Fig. 2b). The electron transfer from NZVI/Cu^0 to O_2 stimulated the production of $O_2^{\bullet-}$ radical, which further took part in the generation of $SO_4^{-\bullet}$. The $O_2^{\bullet-}$ radical as well as the electron transfer from NZVI/Cu^0 to Fe(III)/Cu(II) promoted the cycling of Fe(III)/Fe(II) and Cu(II)/Cu(I) (Xu et al., 2024; Fig. 2c).

Fig. 2.

For the aforementioned metal-modified biochars, the reaction between -C=O functional groups in the biochar and HSO_5^- generated $SO_5^{-\bullet}$ through the electron transfer. $^1O_2$ species were produced by the self-decomposition of HSO_5^-, $SO_5^{-\bullet}$ and $SO_4^{-\bullet}$, as well as self-scavenging reaction between $O_2^{\bullet-}$ and ·OH (Xiao et al., 2022; Xu et al., 2024; Fig. 2d). The graphitic N within the carbon matrix of Fe-Ce@N-BC encouraged the formation of positively charge sites favourable for adsorption of negative PMS (HSO_5^-), leading to the generation of $^1O_2$ species (Xiao et al., 2022; Fig. 2d). After four different pathways, MET could even be

mineralised to form small molecular products (e.g., NO_3^-/NO_2^-), CO_2 and H_2O (Xiao et al., 2022; Xu et al., 2024; Fig. 2e).

Solution pH plays a key role in degradation of MET in both metal-modified biochar/PS and metal-modified biochar/PMS systems. Under strong alkaline condition (e.g., pH = 10), the free radicals (i.e., $SO_4^{\cdot-}$) are consumed by OH^- to release ·OH with lower oxidation capability, resulting in declined removal of MET. $SO_4^{\bullet-}$ and ·OH are quenched by excessive H^+ in strong acidic solution (e.g., pH = 3), which decreases the removal rate. Hence, the optimum removal efficiencies of MET can be obtained under weak acidic and/or weak alkaline conditions (e.g., almost 100% in the KMBC/PS system at pH of 6.5-8.0, > 81.8% in Fe-Ce@N-BC/PMS system at pH of 5.74; Luo et al., 2022; Xiao et al., 2022). It should be noted that in the NZVI/Cu^0/BC-3/PMS system, MET could be completely removed at a wide pH range of 3-9. The extremely high pH (pH = 11) caused a slight decline in the removal efficiency, reaching around 94%. This could be due to the rapid production of highly active ROS at a large number on the NZVI/Cu^0/BC-3 at different pH (Xu et al., 2024).

Fe(II) (FeO) in the metal-modified biochar plays a key role in the removal of targeted pollutants (e.g., MET) via Fenton-like degradation. Fe(II) activates H_2O_2 to generate ·OH, which helps to degrade MET (Fig. 3; Yi et al., 2020). The acidic condition (i.e., pH = 3) prompts the release of Fe(II) from the biochar and limits the iron precipitation in the metal-modified biochar/Fenton-like system, encouraging generation of ·OH for degradation of MET (e.g., removal of almost 100% using SMBC and MBC). It should be noted that the pH range favourable for removal of MET is affected by different chemical reagents for preparation of metal-modified biochar. For example, SMBC obtained from immersing biomass powder in diluted steel pickling waste liquor could be used at a wide pH range of 3-11 to realise more than 80% removal of MET. At alkaline condition, SMBC decreased solution pH (i.e., from 11 to 9.56) using H^+ which was previously adsorbed onto the biochar during the preparation

process (Yi et al., 2019; Yi et al., 2020). However, ferric hydroxide complexes would form under strong alkaline condition (e.g., pH = 9-11) when employing MBC derived from biomass mixing with Fe^{2+} solution, which prohibited the formation of ·OH (Yi et al., 2021).

Fig. 3.

During the photo-Fenton process, a single electron transfer mechanism from the metal centre on the magnetic MFe_2O_4@BC can explain the degradation of target pollutants (i.e., MET; Fig. 4). After exciting electrons from valence band (VB) to the conduction band (CB) and generating holes in the VB of the catalysts, H_2O_2, H_2O and OH^- involve in generation of ·OH using photogenerated electrons (e^-) and holes (h^+) (Step 1). In Step 2, for $CoFe_2O_4$@BC, Co(II) activates H_2O_2 to release ·OH radicals and Co(III). The reduction reaction with Co(III) and Fe(II) further generates Fe(III) and Co(II). As to $CuFe_2O_4$@BC, Cu(I) generated from activating H_2O_2 by Cu(II) converts Fe(III) to Fe(II). Fe(III) also reacts with OH^- under UV or visible light illumination to produce ·OH (Step 3). The reaction between Fe(II) and H_2O_2 stimulates generation of ·OH (Step 4). Finally, the generated ·OH reduces MET to degraded products (Step 5). The photo-Fenton process with magnetic $CoFe_2O_4$@BC can be only operated at pH of 3. However, the application of the magnetic $CuFe_2O_4$@BC enables a wide pH range (i.e., 3-7) favourable for the photo-Fenton process as $CuFe_2O_4$ with a narrow bandgap of 1.4 eV can absorb visible light more efficiently and enhance catalytic ability at neutral pH condition (Cai et al., 2021 and 2023).

Fig. 4.

The electrochemical oxidation (ECO) of MET has also been investigated in an electrolysis process using Fe_1:Co_2-bwc/LBE as anode and LBE as cathode, in which ·OH generated from water involved the conversion of MET to small aliphatic and further CO_2,

H_2O and NO_3^- (Sharan et al., 2023; Fig. 5). The weak acid condition (pH = 6.4) or neutral condition (pH = 7) more effectively oxidised MET than strong acidic (pH = 3~5) and alkaline conditions (pH = 9) (Sharan et al., 2023).

Fig. 5.

4. Comparison among different types of advanced biochar-based materials

The modified biochar prepared using pyrolysis and flash heating methods at higher temperature (e.g., 400-950 ºC) possesses higher specific surface area, higher pore volume and abundant functional groups (e.g., -OH, C-O, C=O, C=C, etc.) favourable for adsorption of specific antibiotics. The metal-modified biochar can be prepared at relatively lower pyrolysis temperature (e.g., 180-800 ºC), and be used in both adsorption process and AOP for removal of specific antibiotics. The introduction of metal species embeds the modified biochar with abundant functional groups (e.g., metal-O, C=O, -OH, -COOH, C-O, etc.), enhancing the adsorption ability. The modified biochar is generally employed at a relatively high dosage (Table 2; e.g., 1.0-2.0 g/L) during the adsorption process, which is significantly affected by solution pH related to pH_{pzc} of biochar, and pKa, pKa1, and pKa2 of the antibiotics.

Table 2.

Bimetallic iron-modified biochar has been widely applied in AOP (e.g., PS, PMS, photo-Fenton process, electrochemical oxidation) at a low dosage (e.g., < 1.0 g/L). This type of metal-modified biochar (e.g., MMBC, KMBC, NMBC) possesses high specific surface area with the uniform distribution of iron species, and contains high contents of Fe(II) and reducing functional groups (e.g., O=C, C=C, C≡N, etc.) favourable for activating PS system. The presence of defective graphitic structure in the modified biochar (e.g., NMBC, bimetallic NZVI/Cu^{0}/BC-3 composite) improves the activation of PS and PMS systems. In the PS, PMS,

photo-Fenton process, the release of metal species is limited in the modified biochar via conversion cycle of metal ions at different valence states (e.g., MMBC, Fe-Ce@N-BC, MFe_2O_4@BC), or the formation of a special shell/core structure with the biochar as the protective layer for metal species (e.g., the bimetallic NZVI/Cu^0/BC-3 composite). Moreover, this type of the modified biochar stimulates generation of more ROS due to the involvement of various metal species and the modified biochar with high conductivity and abundant functional groups. The bimetallic iron-modified biochar enables both PMS system and photo-Fenton process to be operated at a wide pH range, e.g., pH range of 3-9 for NZVI/Cu^0/BC-3/PMS system, 3-7 for $CoFe_2O_4$@BC in photo-Fenton process. During the electrochemical oxidation process, the bimetallic iron-modified biochar (e.g., Fe_1:Co_2-bwc/LBE) can improve the conductivity, and provide more surface area for electron mass transfer, thereby increasing release of more ·OH radicals. Regarding final products after removal processes, adsorption of the targeted pollutants on the biochar after adsorption is a major issue as the parent compounds remained on the biochar may lead to secondary pollution. After AOP, the specific antibiotics (e.g., MET) could be mineralised to form small molecular products (e.g., NO_3^-/NO_2^-), CO_2 and H_2O.

Overall, the metal-modified biochar, especially bimetallic iron-modified biochar, is the most suitable modified biochar for removal of specific antibiotics via AOP.

5. Future research perspectives

The modified biochar prepared at high pyrolysis temperature have to be regenerated by using chemical reagents such as HCl solution, NaOH solution, etc. The strong acid or alkaline solution used may induce secondary pollution. Moreover, the high pyrolysis temperature may cause high energy requirement and operational cost. The reusability of the metal-modified biochar has not yet been frequently investigated in the adsorption and AOP

system. pH_{pzc} of biochar is substantially influenced by solution pH, which further affects the adsorption of targeted pollutants. Moreover, pH also needs to be optimised in the metal-modified biochar-assisted AOP to realise effective degradation process. Most of the studies regarding removal of specific antibiotics by the modified biochar are mainly carried out in the lab scale. Therefore, more research is needed in the future as follows:

1) More novel biochar needs to be developed at relatively low pyrolysis temperature to save energy and cost. Additionally, it requires to explore environmental-friendly chemical reagents for regeneration of the modified biochar as an alternative for strong acidic or alkaline solution.
2) For the adsorption process, the metal-modified biochar can be prepared using metal ions-containing solution including chloride ions (e.g., $FeCl_3$, $FeCl_2$, $ZnCl_2$, $CoCl_2$, etc.) to obtain high specific surface area and pore volume.
3) The preparation of bimetallic iron-modified biochar needs to be realised employing bimetallic ions-containing solution including oxide species, such as nitrate ions (e.g., $Fe(NO_3)_3$, $Cu(NO_3)_2$, etc.) and sulphate ions (e.g., $FeSO_4$, $MnSO_4$, etc.), to allow the conversion cycle of metal ions at different valence states. This limits the release of metal ions and further enables the effective activation of AOP and more generation of ROS for degradation of the specific antibiotics. Moreover, the metal-modified biochar obtained should have the ability to minimise the effects of pH on the removal efficiencies.
4) Nitrogen doping with exogeneous nitrogen, and modifying using more types of clays or zeolites can be explored to further improve the properties of metal-modified biochar (e.g., formation of extra active sites including the pyrrolic-N and graphitic-N, higher ion exchange ability, etc.) for adsorption, as well as to increase the capability of the modified biochar in activating AOP.

5) The stability and reusability of metal-modified biochar should be investigated when employing in adsorption process and AOP system under different operational conditions (e.g., solution pH, dosage, etc.). Moreover, it also needs to explore the circular economy-based approaches for disposal of the metal-modified biochar at the end of experiments.
6) The studies on the application of the metal-modified biochar can be extended into the removal of a wide range of specific antibiotics in more depth in terms of properties of biochar and targeted antibiotics, factors influencing the removal of the antibiotics, removal mechanisms and identification of final products after removal processes.
7) Large-scale applications of newly developed biochar will be another focus in the future study with respect to removal of specific antibiotics from hospital wastewater. It also should carry out the techno-economic analysis and circular economy-based assessment of the biochar and the whole process.

6. Conclusions

This review highlights the properties of advanced biochar-based materials used for eliminating specific antibiotics from hospital wastewater and removal mechanisms. The modified biochar obtained at higher pyrolysis temperature have large specific surface area, high pore volume and abundant functional groups favourable for the adsorption process. Metal-modified biochar contains abundant functional groups and defective graphitic structure, inhibits leaching of metal ions, and increases separation rate of electron-hole pairs. The metal-modified biochar not only enhances adsorption of the targeted pollutants, but also has the excellent ability in activating AOS to generate more ROS. Adsorption mechanisms mainly depend on the pyrolysis temperature, solution pH and characteristics of modified biochar and targeted pollutants. In the PS and PMS systems with the metal-modified biochar, weak acidic and alkaline conditions favour the removal of targeted pollutants (e.g., pH of 5.7-

8.0 for removal of MET). Nevertheless, the NZVI/Cu^0/BC-3/PMS system can widen the operational pH range to 3-9. The effective removal of pollutants in Fenton-like process can be achieved at a broad pH range (e.g., pH of 3-11 for removal of MET) when using SMBC with the ability of releasing H^+ under alkaline condition. The metal-modified biochar with a narrow bandgap allows more efficient absorption of visible light during the photo-Fenton degradation of MET, which extends the operational pH from 3 to 7. The ECO using Fe_1:Co_2-bwc/LBE as anode is better to be operated under weak acid condition (pH = 6.4) or neutral condition (pH = 7). Future research needs to step in developing novel metal-modified biochar with high potential in limiting effects of pH on the removal processes and eliminating a wide range of specific antibiotics.

References

Ajala, O.J., Tijani, J.O., Salau, R.B., Abdulkareem, A.S., Aremu, O.S., 2022. A review of emerging micro-pollutants in hospital wastewater: Environmental fate and remediation options. Results Eng. 16, 100671. https://doi.org/10.1016/j.rineng.2022.100671

Ameen, F., Mostafazadeh, R., Hamidian, Y., Erk, N., Sanati, A.L., Karaman, C., Ayati, A., 2023. Modeling of adsorptive removal of azithromycin from aquatic media by $CoFe_2O_4$/NiO anchored microalgae-derived nitrogen-doped porous activated carbon adsorbent and colorimetric quantifying of azithromycin in pharmaceutical products. Chemosphere 329, 138635. https://doi.org/10.1016/j.chemosphere.2023.138635

Anuar, N.F., Shah, D.R.S.I., Ramli, F.F., Zaini, M.S.M., Mohammadi, N.A., Daud, A.R.M., Syed-Hassan, S.S.A., 2023. The removal of antibiotics in water by chemically modified

carbonaceous adsorbents from biomass: A systematic review. J. Clean Prod. 401, 136725. https://doi.org/10.1016/j.jclepro.2023.136725

Arif, M., Liu, G., Rehman, M.Z.ur, Mian, M.M., Ashraf, A., Yousaf, B., Rashid, M.S., Ahmed, R., Imran, M., Munir, M.A.M., 2023. Impregnation of biochar with montmorillonite and its activation for the removal of azithromycin from aqueous media. Environ. Sci. Pollut. Res. 30, 78279–78293. https://doi.org/10.1007/s11356-023-27908-z

Aydin, S., Aydin, M.E., Ulvi A., Kilic, H., 2018. Antibiotics in hospital effluents: occurrence, contribution to urban wastewater, removal in a wastewater treatment plant, and environmental risk assessment. Environ. Sci. Pollut. Res. 26, 544–558. https://doi.org/10.1007/s11356-018-3563-0

Aydın, S., Bedük, F., Ulvi, A., Aydın, M.E., 2021. Simple and effective removal of psychiatric pharmaceuticals from wastewater treatment plant effluents by magnetite red mud nanoparticles. Sci. Total Env. 784, 147174. https://doi.org/10.1016/j.scitotenv.2021.147174

Azalok, K.A., Oladipo, A.A., Gazi, M., 2021. Hybrid MnFe-LDO-biochar nanopowders for degradation of metronidazole via UV-light-driven photocatalysis: Characterization and mechanism studies. Chemosphere 268, 128844. https://doi.org/10.1016/j.chemosphere.2020.128844

Azeez, L., Adefunke, O., Oyedeji, A.O., Agbaogun, B.K., Busari, H.K., Adejumo, A.L., Agbaje, W.B., Adeleke, A.E., Samuel, A.O., 2024. Facile removal of rhodamine B and metronidazole with mesoporous biochar prepared from palm tree biomass: adsorption studies, reusability, and mechanisms. Water Pract. Technol. 19 (3), 730–744. https://doi.org/10.2166/wpt.2024.049

Aziz, S., Anbreen, S., Iftikhar, I., Fatima, T., Iftikhar, A., Ali, L., 2024. Green technology: synthesis of iron-modified biochar derived from pine cones to remove azithromycin and ciprofloxacin from water. Front. Environ. Sci. 12,1353267. https://doi.org/10.3389/fenvs.2024.1353267

Balarak, D., Mahvi, A.H., Shahbaksh, S., Wahab, M.A., Abdala, A., 2021. Adsorptive Removal of Azithromycin Antibiotic from Aqueous Solution by Azolla Filiculoides-Based Activated Porous Carbon. Nanomaterials 11(12), 3281. https://doi.org/10.3390/nano11123281

Bai, H., Zhang, Q., Zhou, X., Chen, J., Chen, Z., Liu, Z., Yan, J., Wang, J., 2023. Removal of fluoroquinolone antibiotics by adsorption of dopamine-modified biochar aerogel. Korean J. Chem. Eng. 40, 215–222. https://doi.org/10.1007/s11814-022-1263-4

Boillot, C., C. Bazin, F. Tissot-Guerraz, J. Droguet, M. Perraud, J.C. Cetre, D. Trepo, Y. Perrodin, 2008. Daily physicochemical, microbiological and ecotoxicological fluctuations of a hospital effluent according to technical and care activities. Sci. Total Environ. 403(1-3), 113-129. https://doi.org/10.1016/j.scitotenv.2008.04.037

Byju's, 2024. What is pKa?, https://byjus.com/chemistry/pka/ (accessed 18 January 2024)

Cai, H., Ma, Z., Zhao, T., 2021. Fabrication of magnetic $CuFe_2O_4$@PBC composite and efficient removal of metronidazole by the photo-Fenton process in a wide pH range. J. Environ. Manage. 300, 113677. https://doi.org/10.1016/j.jenvman.2021.113677

Cai, M., Wang, Z., Gu, H., Dong, H., Zhang, X., Cui, N., Zhou, L., Chen, G., Zou, G., 2022a. Occurrence and temporal variation of antibiotics and antibiotic resistance genes in hospital inpatient department wastewater: Impacts of daily schedule of inpatients and wastewater treatment process. Chemosphere 292, 133405. https://doi.org/10.1016/j.chemosphere.2021.133405

Cai, H., Zhang, D., Ma, X., Ma, Z., 2022b. A novel ZnO/biochar composite catalysts for visible light degradation of metronidazole. Sep. Purif. Technol. 288, 120633. https://doi.org/10.1016/j.seppur.2022.120633

Cai, Hao, Zhao, T., Ma, Z., 2023. Synthesis of magnetic MFe_2O_4@PC (M = Fe, Cu, Co, and Mn) composites and application of heterogeneous photo-Fenton efficient removal of metronidazole under visible light. J. Ind. Eng. Chem. 121, 322–330. https://doi.org/10.1016/j.jiec.2023.01.035

Calisto, V., Ferreira, C.I.A., Oliveira, J.A.B.P., Otero, M., Esteves, V.I., 2015. Adsorptive removal of pharmaceuticals from water by commercial and waste-based carbons. J. Environ. Manage. 152, 83-90. https://doi.org/10.1016/j.jenvman.2015.01.019

Calisto, V., Jaria, G., Silva, C.P., Ferreira, C.I.A., Otero, M., Esteves, V.I., 2017. Single and multi-component adsorption of psychiatric pharmaceuticals onto alternative and commercial carbons. J. Environ. Manage. 192, 15-24. https://doi.org/10.1016/j.jenvman.2017.01.029

Chebbi, M., Ounoki, S., Youcef, L., Amrane, A., 2023. Synthesis and characterization of pine cones biochar for the removal of an antibiotic (Metronidazole) from aqueous solutions. J. Ind. Eng. Chem. 126, 327-339. https://doi.org/10.1016/j.jiec.2023.06.023

Ding, Z., Ge, Y., Gowd, S.C., Singh, E., Kumar, V., Chaurasia, D., Kumar, V., Rajendran, K., Bhargava, P.C., Wu, P., Lin, F., Harirchi, S., kumar, V.A., Sirohi, R., Sindhu, R., Binod, P., Taherzadeh, M.J., Awasthi, M.K., 2023. Production of biochar from tropical fruit tree residues and ecofriendly applications – A review. Bioresour. Technol. 376, 128903. https://doi.org/10.1016/j.biortech.2023.128903

Du, L., Ahmad, S., Liu, L., Wang, L., Tang, J., 2023. A review of antibiotics and antibiotic resistance genes (ARGs) adsorption by biochar and modified biochar in water. Sci. Total Environ. 858, 159815. https://doi.org/10.1016/j.scitotenv.2022.159815

Fatimazahra, S., Latifa, M., Laila, S., Monsif, K., 2023. Review of hospital effluents: special emphasis on characterization, impact, and treatment of pollutants and antibiotic resistance. Environ. Monit. Assess. 195, 393. https://doi.org/10.1007/s10661-023-11002-5

Feng, Z., Zhai, X., Sun, T., 2022. Sustainable and efficient removal of paraben, oxytetracycline and metronidazole using magnetic porous biochar composite prepared by one step pyrolysis. Sep. Purif. Technol. 293, 121120. https://doi.org/10.1016/j.seppur.2022.121120

Gao, T., Shi, W., Zhao, M., Huang, Z., Liu, X., Ruan, W., 2022. Preparation of spiramycin fermentation residue derived biochar for effective adsorption of spiramycin from wastewater. Chemosphere 296, 133902. https://doi.org/10.1016/j.chemosphere.2022.133902

Han, S., Wang, Z., Huang, H., Wang, T., Zhou, Z., Bai, Y., Du, P., Li, X., 2022. Estimating antibiotics use in major cities in China through wastewater-based epidemiology. Sci. Total Environ. 826, 154116. https://doi.org/10.1016/j.scitotenv.2022.154116

Herrera, K., Morales, L.F., Tarazona, N.A., Aguado, R., Saldarriaga, J.F., 2022. Use of Biochar from Rice Husk Pyrolysis: Part A: Recovery as an Adsorbent in the Removal of Emerging Compounds. ACS Omega 7, 7625−7637. https://doi.org/10.1021/acsomega.1c06147

Herrera, K., Morales, L.F., López, J.E., Montoya-Ruiz, Carolina, Muñoz, S., Zapata, D., Saldarriaga, J.F., 2023. Biochar production from tannery waste pyrolysis as a circular economy strategy for the removal of emerging compounds in polluted waters. Biomass Conv. Bioref. https://doi.org/10.1007/s13399-023-04261-2

Helmenstine, A.M., 2019. Acid Dissociation Constant Definition: Ka. https://www.thoughtco.com/acid-dissociation-constant-definition-ka-606347 (accessed 18 January 2024)

Hu, T., Liu, J., Fang, Y., Feng, N., Wang, G., Tong, J., Lu, K., Yang, Q., Ma, W., Wu, H., Xie, J., 2024. Preparation of a microbial char adsorbent from polyethyleneimine-modified and nickel-loaded microorganisms for efficient removal of metronidazole. Environ. Sci.: Water Res. Technol. 10, 588-602. https://doi.org/10.1039/D3EW00752A

Katiyar, R., Chen, C.W., Singhania, R.R., Tsai, M.L., Saratale, G.D., Pandey, A., Cheng-Dong, D., Patel, A.K., 2022. Efficient remediation of antibiotic pollutants from the environment by innovative biochar: current updates and prospects. Bioengineered 13(6), 14730-14748. https://doi.org/10.1080/21655979.2022.2108564

Krasucka, P., Pan, B., Ok, Y.S., Mohan, D., Sarkar, B., Oleszczuk, P., 2021. Engineered biochar – A sustainable solution for the removal of antibiotics from water. Chem. Eng. J. 405, 126926. https://doi.org/10.1016/j.cej.2020.126926

Jaria, G., Lourenço, M.A.O., Silva, C.P., Ferreira, P., Otero, M., Calisto, V., Esteves, V.I., 2020. Effect of the surface functionalization of a waste-derived activated carbon on pharmaceuticals' adsorption from water. J. Mol. Liq. 299, 112098. https://doi.org/10.1016/j.molliq.2019.112098

Lien, L.T.Q., Hoa, N.Q., Chuc, N.T.K., Thoa, N.T.M., Phuc, H.D., Diwan, V., Dat, N.T., Tamhankar, A.J., Lundborg, C.S., 2016. Antibiotics in Wastewater of a Rural and an Urban Hospital before and after Wastewater Treatment, and the Relationship with Antibiotic Use—A One Year Study from Vietnam. Int. J. Environ. Res. Public Health 13, 588. https://doi.org/10.3390/ijerph13060588

Liu, J., Jiang, J., Meng, Y., Aihemaiti, A., Xu, Y., Xiang, H., Gao, Y., Chen, X., 2020. Preparation, environmental application and prospect of biochar-supported metal

nanoparticles: A review. J. Hazard. Mater. 388, 122026. https://doi.org/10.1016/j.jhazmat.2020.122026

Liu, T., Cui, K., Li, C.X., Chen, Y., Wang, Q., Yuan, X., Chen, Y., Liu, J., Zhang, Q., 2023. Efficient peroxymonosulfate activation by biochar-based nanohybrids for the degradation of pharmaceutical and personal care products in aquatic environments. Chemosphere 311, 137084. https://doi.org/10.1016/j.chemosphere.2022.137084

Luo, J., Yi, Y., Ying, G., Fang, Z., Zhang, Y., 2022. Activation of persulfate for highly efficient degradation of metronidazole using Fe(II)-rich potassium doped magnetic biochar. Sci. Total Environ. 819, 152089. https://doi.org/10.1016/j.scitotenv.2021.152089

Luo, J., Yi, Y., Fang, Z., 2023a. Effect of Mn-based magnetic biochar /PS reaction system on oxidation of metronidazole. Chemosphere 332, 138747. https://doi.org/10.1016/j.chemosphere.2023.138747

Luo, J., Yi, Y., Fang, Z., 2023b. Nitrogen-rich magnetic biochar prepared by urea was used as an efficient catalyst to activate persulfate to degrade organic pollutants. Chemosphere 339, 139614. https://doi.org/10.1016/j.chemosphere.2023.139614

Mahari, W.A.W., Waiho, K., Azwar, E., Fazhan, H., Peng, W., Ishak, S.D., Tabatabaei, M., Yek, P.N.Y., Almomani, F., Aghbashlo, M., Lam, S.S., 2022. A state-of-the-art review on producing engineered biochar from shellfish waste and its application in aquaculture wastewater treatment. Chemosphere 288, 132559. https://doi.org/10.1016/j.chemosphere.2021.132559

Manjunath, S.V., Kumar, Mathava, 2018. Evaluation of single-component and multi-component adsorption of metronidazole, phosphate and nitrate on activated carbon from Prosopıs julıflora. Chem. Eng. J. 346, 525–534. https://doi.org/10.1016/j.cej.2018.04.013

Moratalla, Á., Cotillas, S., Lacasa, E., Fernández-Marchante, C.M., Ruiz, S., Valladolid, A., Cañizares, P., Rodrigo, M., Saez, C., 2022. Occurrence and toxicity impact of pharmaceuticals in hospital effluents: Simulation based on a case of study. Process Saf. Environ. Prot. 168, 10–21. https://doi.org/10.1016/j.psep.2022.09.066

Nasiri, A., Heidari, M.R., Javid, N., Yazdanpanah, G., 2022. New efficient and recyclable magnetic nanohybrid adsorbent for the metronidazole removal from simulated wastewater. J. Mater. Sci.: Mater. Electron 33, 25103–25126. https://doi.org/10.1007/s10854-022-09216-3

Ngigi, A.N., Magu, M.M., Muendo B.M., 2020. Occurrence of antibiotics residues in hospital wastewater, wastewater treatment plant, and in surface water in Nairobi County, Kenya. Environ. Monit. Assess. 192,18. https://doi.org/10.1007/s10661-019-7952-8

Omuferen, L.O., Maseko, B., Olowoyo, J.O., 2022. Occurrence of antibiotics in wastewater from hospital and convectional wastewater treatment plants and their impact on the effluent receiving rivers: current knowledge between 2010 and 2019. Environ. Monit. Assess. 194, 306. https://doi.org/10.1007/s10661-022-09846-4

Ouyang, J., Zhou, L., Liu, Z., Heng, J.Y.Y., Chen, W., 2020. Biomass-derived activated carbons for the removal of pharmaceutical mircopollutants from wastewater: A review. Sep. Purif. Technol. 253, 117536. https://doi.org/10.1016/j.seppur.2020.117536

Pariente, M.I., Segura, Y., Álvarez-Torrellas, S., Casas, J.A., de Pedro, Z.M., Diaz, E., García, J., López-Muñoz, M.J., Marugán, J., Mohedano, A.F., Molina, R., Munoz, M., Pablos, C., Perdigón-Melón, J.A., Petre, A.L., Rodríguez, J.J., Tobajas, M., Martínez, F., 2022. Critical review of technologies for the on-site treatment of hospital wastewater: From conventional to combined advanced processes. J. Environ. Manage. 320, 115769. https://doi.org/10.1016/j.jenvman.2022.115769

Segura, Y., del Álamo, A.C., Munoz, M., Álvarez-Torrellas, S., García, J., Casas, J.A., De Pedro, Z.M., Martínez, F., 2021. A comparative study among catalytic wet air oxidation, Fenton, and Photo-Fenton technologies for the on-site treatment of hospital wastewater. J. Environ. Manage. 290, 112624. https://doi.org/10.1016/j.jenvman.2021.112624

Sharan, S., Khare, P., Shankar, R., Mishra, N.K., Tyagi, A., 2023. Bimetal-oxide (Fe/Co) modified bagasse-waste carbon coated on lead oxide-battery electrode for metronidazole removal. J. Environ. Manage. 347, 119104. https://doi.org/10.1016/j.jenvman.2023.119104

Stylianou, M., Christou, A., Michael, C., Agapiou, A., Papanastasiou, P., Fatta-Kassinos, D., 2021. Adsorption and removal of seven antibiotic compounds present in water with the use of biochar derived from the pyrolysis of organic waste feedstocks. J. Environ. Chem. Eng. 9(5), 105868. https://doi.org/10.1016/j.jece.2021.105868

Suarez, S., Juan M. Lema, Francisco Omil, 2009. Pre-treatment of hospital wastewater by coagulation–flocculation and flotation. Bioresour. Technol. 100(7), 2138–2146. https://doi.org/10.1016/j.biortech.2008.11.015

Sun, L., Chen, D., Wan, S., Yu, Z., 2018. Adsorption Studies of Dimetridazole and Metronidazole onto Biochar Derived from Sugarcane Bagasse: Kinetic, Equilibrium, and Mechanisms. J. Polym. Environ. 26, 765-777. https://doi.org/10.1007/s10924-017-0986-5

Szekeres, E., Baricz, A., Chiriac, C.M., Farkas, A., Opris, O., Soran, M.L., Andrei, A.-S., Rudi, K., Balcázar, J.L., Dragos, N., Coman, C., 2017. Abundance of antibiotics, antibiotic resistance genes and bacterial community composition in wastewater effluents from different Romanian hospitals. Environ. Pollut. 225, 304-315. https://doi.org/10.1016/j.envpol.2017.01.054

Tahiri, V., Denaj, A., Prenga, D., 2023. Assessment of the Presence of Pharmaceutical Compounds in Wastewaters and in Aquatic Environment. J. Hum. Earth, Future 4, 2023. https://doi.org/10.28991/HEF-2023-04-03-03

Top, S., Akgün, M., Kıpçak, E., Bilgili, M.S., 2020. Treatment of hospital wastewater by supercritical water oxidation process. Water Res. 185, 116279. https://doi.org/10.1016/j.watres.2020.116279

Ulvi, A., Aydın S., Aydın, M.E., 2022. Fate of selected pharmaceuticals in hospital and municipal wastewater effluent: occurrence, removal, and environmental risk assessment. Environ. Sci. Pollut. Res. 29, 75609–75625. https://doi.org/10.1007/s11356-022-21131-y

Vrchovecká, S., Asatiani, N., Antoš, V., Wacławek, S., Hrabák, P., 2023. Study of Adsorption Efficiency of Lignite, Biochar, and Polymeric Nanofibers for Veterinary Drugs in WWTP Effluent Water. Water Air Soil Pollut. 234, 268. https://doi.org/10.1007/s11270-023-06281-0

Wan, S., Hua, Z., Sun, L., Bai, X., Liang, L., 2016. Biosorption of nitroimidazole antibiotics onto chemically modified porous biochar prepared by experimental design: Kinetics, thermodynamics, and equilibrium analysis. Process Saf. Environ. Prot. 104, 422-435. https://doi.org/10.1016/j.psep.2016.10.001

Wang, J., Lu, X., Jing, Q., Zhang, B., Ye, J., Zhang, H., Xiao, Z., Zhang, J., 2023. Spatiotemporal characterization of heavy metal and antibiotics in the Pearl River Basin and pollutants removal assessment using invasive species-derived biochars. J. Hazard. Mater. 454, 131409. https://doi.org/10.1016/j.jhazmat.2023.131409

Wu, Q., Zhang, Y., Cui, M.H., Liu, H., Liu, H., Zheng, Z., Zheng, W., Zhang, C., Wen, D., 2022. Pyrolyzing pharmaceutical sludge to biochar as an efficient adsorbent for deep removal of fluoroquinolone antibiotics from pharmaceutical wastewater: Performance

and mechanism. J. Hazard. Mater. 426, 127798. https://doi.org/10.1016/j.jhazmat.2021.127798

Xiao, K., Liang, F., Liang, J., Xu, W., Liu, Z., Chen, B., Jiang, X., Wu, X., Xu, J., Beiyuan, J., Wang, H., 2022. Magnetic bimetallic Fe, Ce-embedded N-enriched porous biochar for peroxymonosulfate activation in metronidazole degradation: Applications, mechanism insight and toxicity evaluation. Chem. Eng. J. 433, 134387. https://doi.org/10.1016/j.cej.2021.134387

Xu, L., Wu, C., Chai, C., Cao, S., Bai, X., Ma, K., Jin, X., Shi, X., Jin, P., 2022. Adsorption of micropollutants from wastewater using iron and nitrogen co-doped biochar: Performance, kinetics and mechanism studies. J. Hazard. Mater. 424, 127606. https://doi.org/10.1016/j.jhazmat.2021.127606

Xu, W., Liang, J., Li, J., Pillai, S.C., Liang, F., Li, M., Xiao, K., Li, J., Wang, Y., Jiang, X., Liu, Z., Beiyuan, J., Wang, H., 2024. Biochar encapsulated metal nanoflowers for high efficient degradation of metronidazole via peroxymonosulfate activation. Sep. Purif. Technol. 328, 125081. https://doi.org/10.1016/j.seppur.2023.125081

Yao, S., Ye, J., Yang, Q., Hu, Y., Zhang, T., Jiang, L., Munezero, S., Lin, K., Cui, C., 2021. Occurrence and removal of antibiotics, antibiotic resistance genes, and bacterial communities in hospital wastewater. Environ. Sci. Pollut. Res. 28, 57321–57333. https://doi.org/10.1007/s11356-021-14735-3

Yi, Y., Tu, G., Zhao, D., Tsang, P.E., Fang, Z., 2019. Pyrolysis of different biomass pre-impregnated with steel pickling waste liquor to prepare magnetic biochars and their use for the degradation of metronidazole. Bioresour. Technol. 289, 121613. https://doi.org/10.1016/j.biortech.2019.121613

Yi, Y., Tu, G., Zhao, D., Tsang, P.E., Fang, Z., 2020. Insight into the influence of pyrolysis temperature on Fenton-like catalytic performance of magnetic biochar. Chem. Eng. J. 380, 122518. https://doi.org/10.1016/j.cej.2019.122518

Yi, Y., Luo, J., Fang, Z., 2021. Magnetic biochar derived from Eichhornia crassipes for highly efficient Fenton-like degradation of antibiotics: Mechanism and contributions. J. Environ. Chem. Eng. 9(5), 106258. https://doi.org/10.1016/j.jece.2021.106258

Yurtay, A., Kılıç, M., 2023. Biomass-based activated carbon by flash heating as a novel preparation route and its application in high efficiency adsorption of metronidazole. Diam. Relat. Mater. 131, 109603. https://doi.org/10.1016/j.diamond.2022.109603

Zhang, X., Bhattacharya, T., Wang, C., Kumar, A., Nidheesh, P.V., 2023a. Straw-derived biochar for the removal of antibiotics from water: Adsorption and degradation mechanisms, recent advancements and challenges. Environ. Res. 237, 116998. https://doi.org/10.1016/j.envres.2023.116998

Zhang, X., Zhen, D., Liu, F., Chen, R., Peng, Q., Wang, Z., 2023b. An achieved strategy for magnetic biochar for removal of tetracyclines and fluoroquinolones: Adsorption and mechanism studies. Bioresour. Technol. 369, 128440. https://doi.org/10.1016/j.biortech.2022.128440

Zhang, X., Wei, J., Wang, C., Wang, L., Guo, Z., Song, Y., 2024. Recent advance of Fe-based bimetallic persulfate activation catalysts for antibiotics removal: Performance, mechanism, contribution of the key ROSs and degradation pathways. Chem. Eng. J. 487, 150514. https://doi.org/10.1016/j.cej.2024.150514

Zhou, T., Zhang, Z., Liu, H., Dong, S., Nghiem, L.D., Gao, L., Chaves, A.V., Zamyadi, A., Li, X., Wang, Q., 2023. A review on microalgae-mediated biotechnology for removing pharmaceutical contaminants in aqueous environments: Occurrence, fate, and removal

mechanism. J. Hazard. Mater. 443, 130213.

https://doi.org/10.1016/j.jhazmat.2022.130213

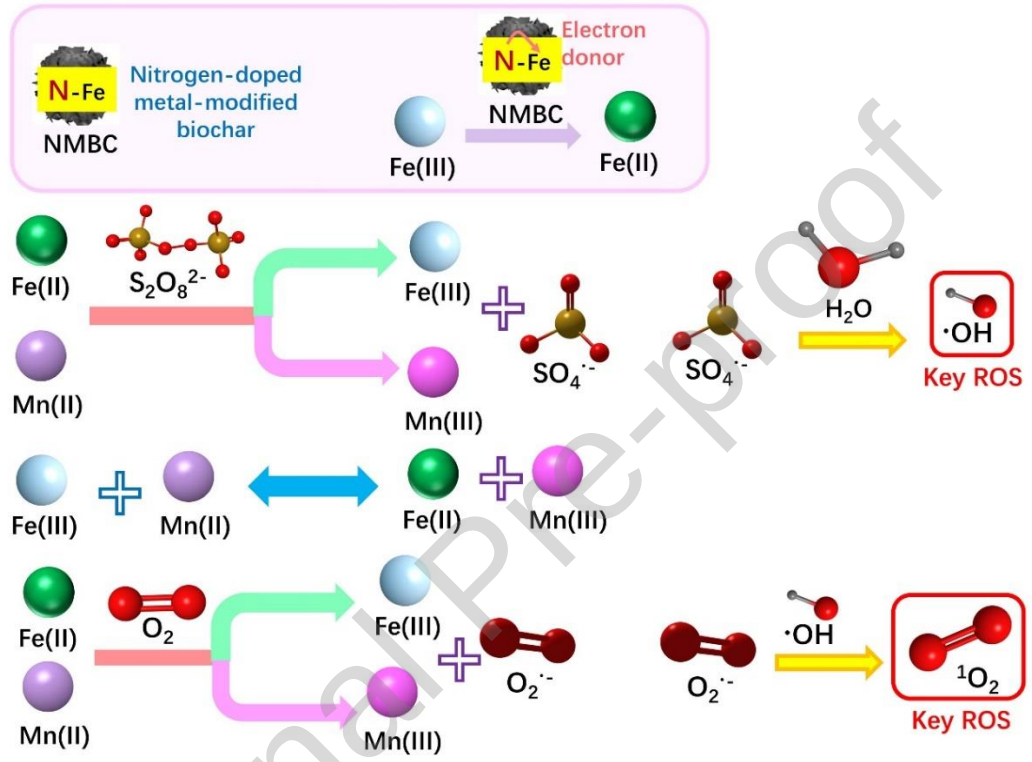

(a)

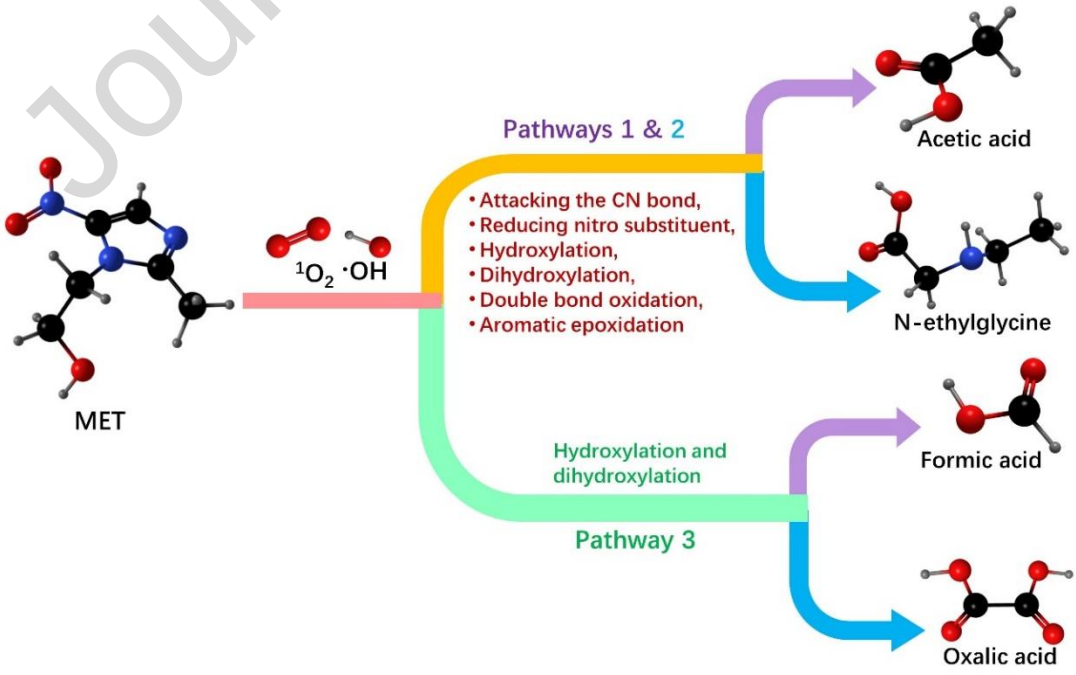

(b)

Fig. 1. Possible pathways for generation of ROS (a) and degradation of MET (b) in metal-modified biochar/PS system

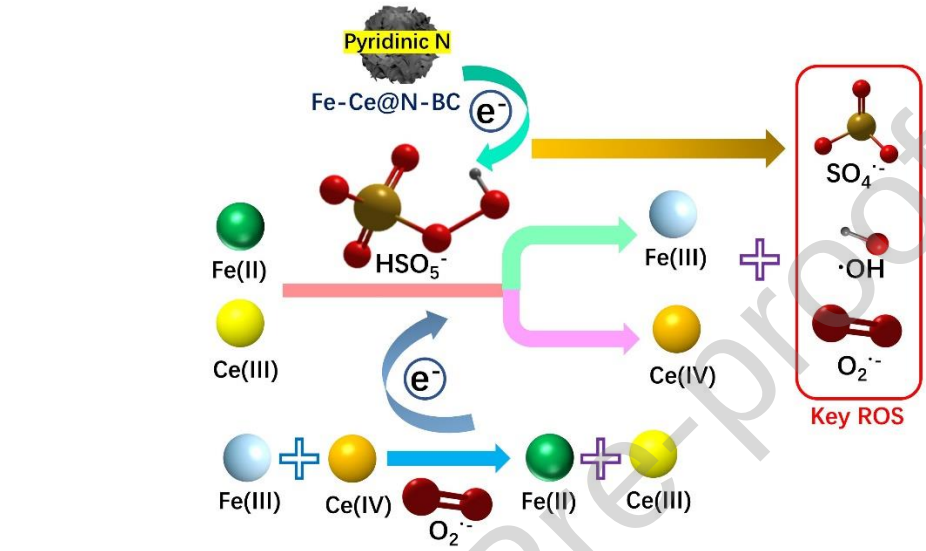

(a)

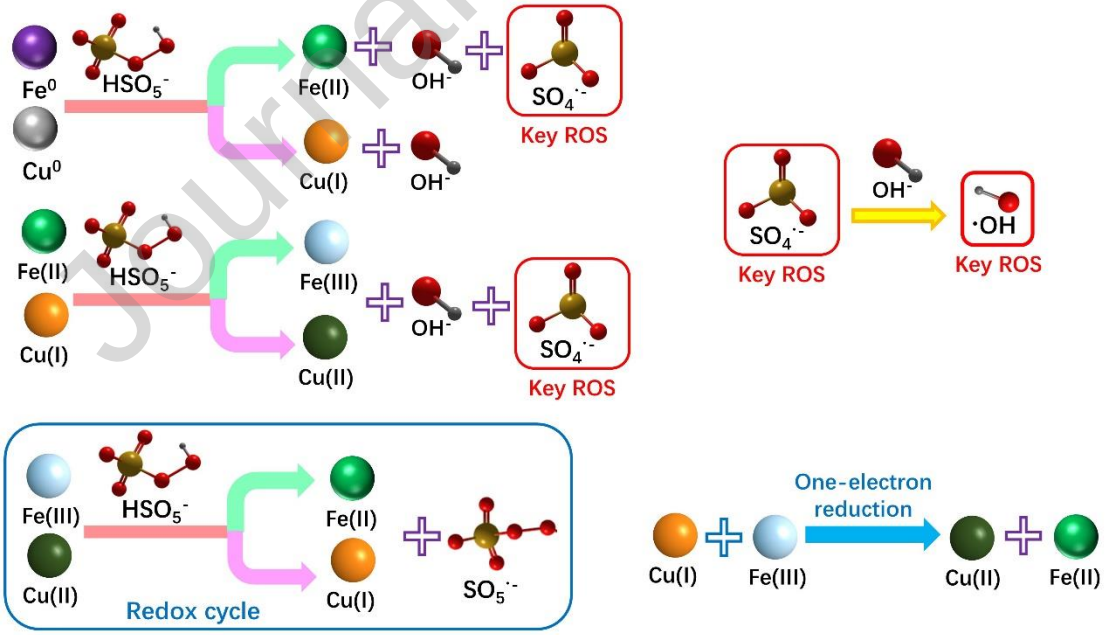

(b)

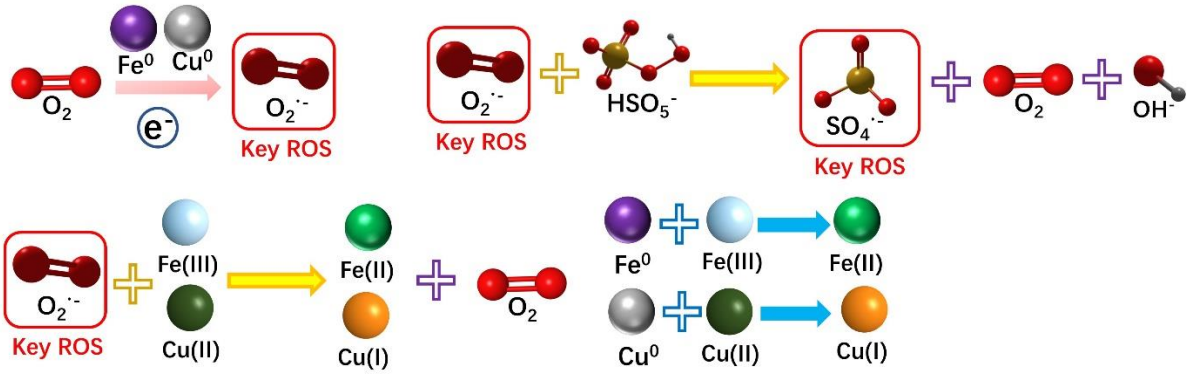

(c)

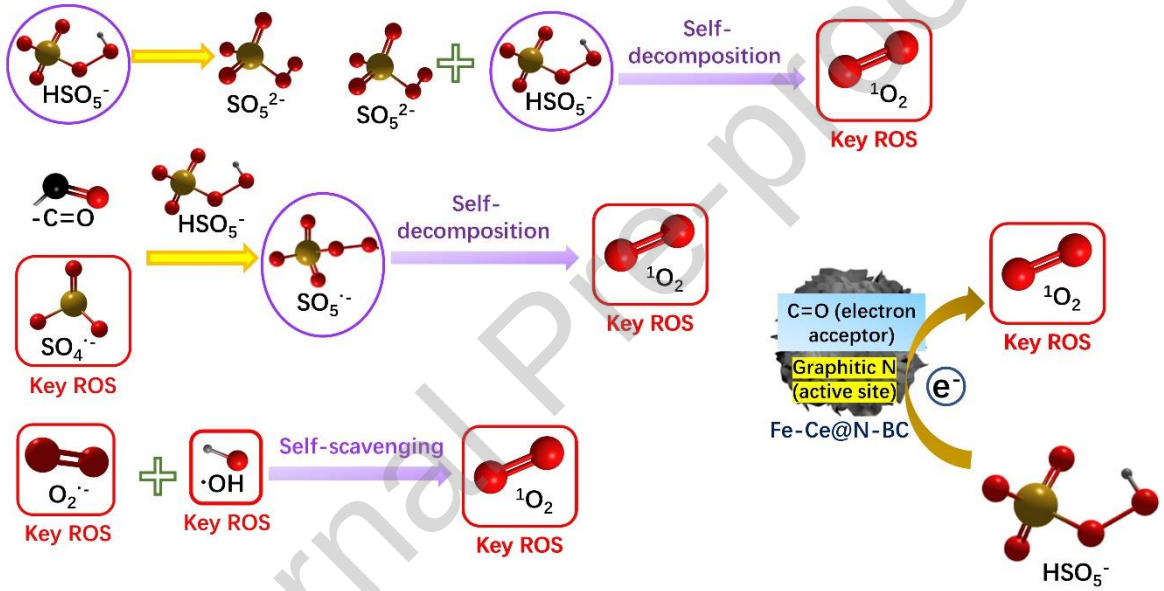

(d)

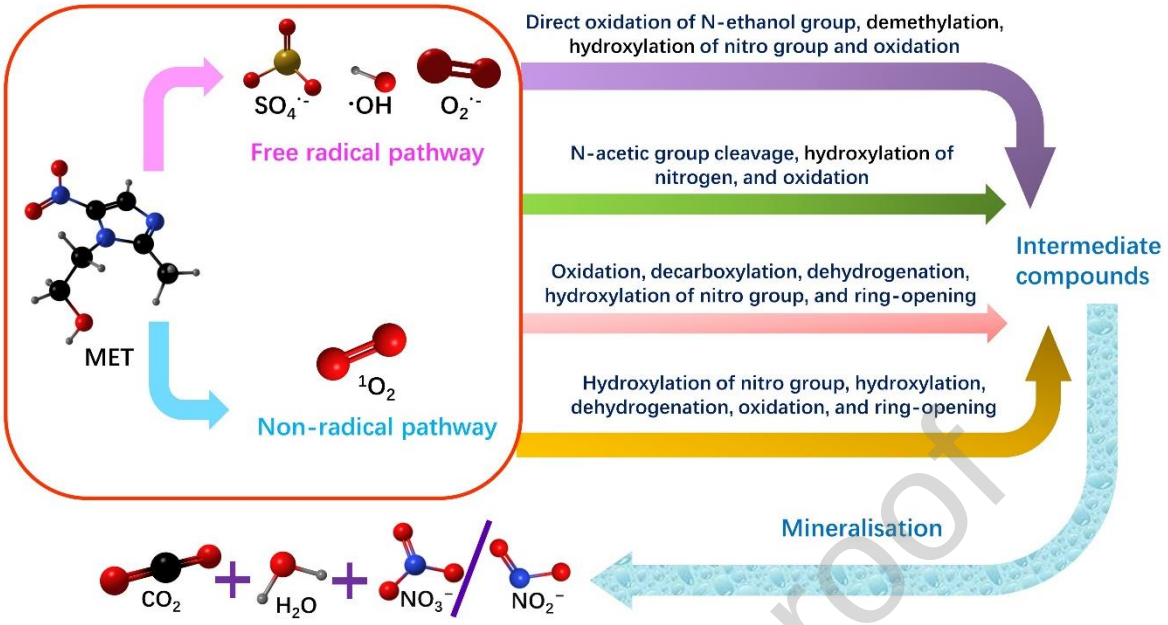

(e)

Fig. 2. Possible pathways for generation of $SO_4^{\cdot-}$, $O_2^{\cdot-}$, and ·OH in the Fe-Ce@N-BC/PMS system (a); for generation of $SO_4^{\cdot-}$, $O_2^{\cdot-}$, and ·OH in the NZVI/Cu^0/BC-3/PMS system (b and c); (d) for generation of $^1O_2$ in the metal-modified biochar/PMS system (d); for degradation of MET in the metal-modified biochar/PMS system (e)

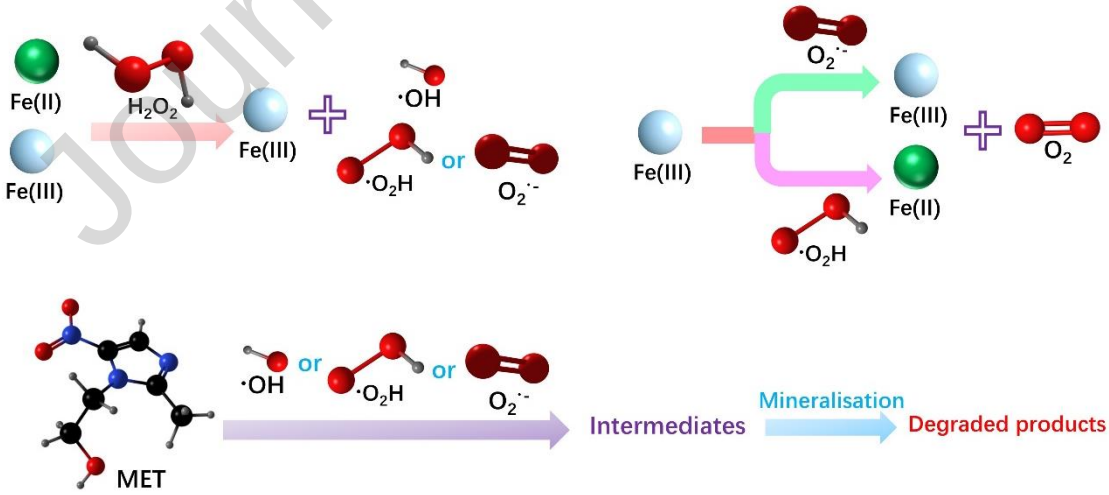

Fig. 3. Possible pathways for generation of ROS and degradation of MET in metal-modified biochar/Fenton-like system

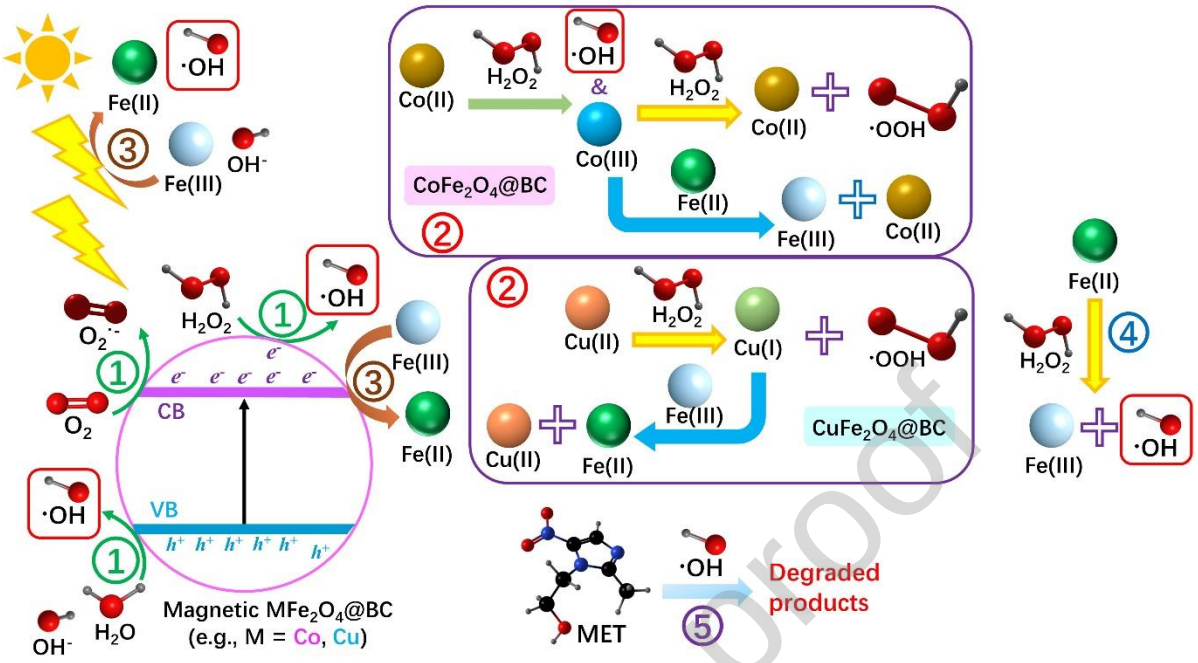

Fig. 4. Possible pathways for generation of ROS and degradation of MET in metal-modified biochar/photo-Fenton process

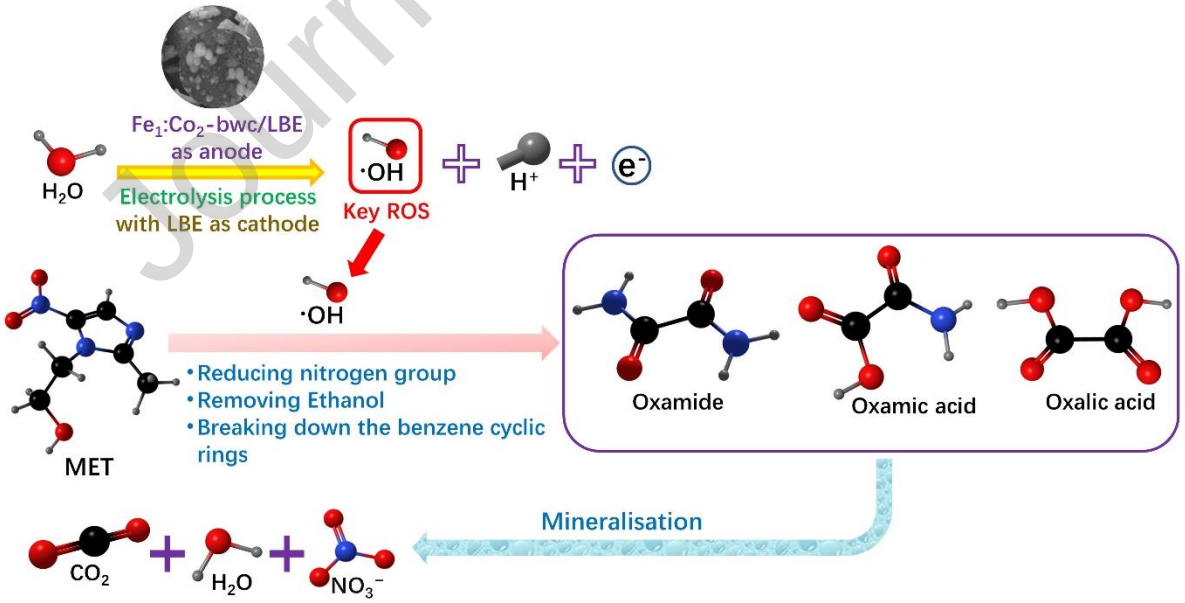

Fig. 5. Possible pathways for the electrochemical oxidation of MET using Fe_1:Co_2-bwc/LBE

Table 1. Biochar-based products for removal of specific antibiotics

Targeted antibiotics	Biochar-based products and their properties[a]	Removal mechanisms	Adsorption isotherm models and kinetic models	Removal performance (removal efficiency (%) or maximum adsorption capacity (mg/g))	References
Clarithromycin (CLA)	• BDB, • SCGDB	• Adsorption	• Freundlich adsorption isotherm	80-100% (1 g/L biochar)	Stylianou et al., 2021
	• Biochar (being prepared by mixing digestate from a biogas plant with agricultural harvests of annual and biennial plants at a ratio of 40%:60%, followed by pyrolyzing at 570 ºC) • SSA, 368.80 m^2/g	• Adsorption	• Langmuir isotherm	34.92 mg/g (1.67 g/L of biochar)	Vrchovecká et al., 2023
Azithromycin (AZM)	• AMBC • Higher SSA of 127 m^2/g and porosity (N_2 adsorption, 17.37 cm^3/g) than those of the pristine biochar (74 m^2/g and 71.58 cm^3/g)	• Adsorption • Endothermic and spontaneous process	• Langmuir and Sips adsorption isotherms; • Pseudo-second-order and Elovich kinetic models	44.73 mg/g (vs 33.4 mg/g with pristine biochar at 1 g/L of biochar)	Arif et al., 2023
	• Rice husk biomass-derived biochar (being prepared at pyrolysis temperature of 450, 500, 550 and 600 ºC); • Higher SSA of 774.83 m^2/g at 500 ºC than those at 450,	• Adsorption	• Langmuir isotherm; • Pseudo-first-order kinetics	> 95%; 612.22 mg/g with biochar obtained at 500 ºC (vs 494-604 mg/g with biochar at	Herrera et al., 2022

	550 and 600 ºC (647-704 m^2/g); • Higher micropore volume of 0.354 cm^3/g at 500 ºC vs 0.214-0.345 cm^3/g at 450, 550 and 600 ºC			450, 550 and 600 ºC)	
	• Tannery hair biochar (being prepared by pyrolysis at 450 ºC, mixing with KOH solution, and carbonizing at 200 ºC under the nitrogen condition) • SSA, 1930 m^2/g	• Adsorption	• The Freundlich model and the Langmuir model	94% (> 250 mg/g at 0.5 g/L biochar)	Herrera et al., 2023
	• Biochar (being prepared by mixing digestate from a biogas plant with agricultural harvests of annual and biennial plants at a ratio of 40%:60%, followed by pyrolyzing at 570 ºC) • SSA, 368.80 m^2/g	• Adsorption	• Langmuir isotherm	34.80 mg/g (1.67 g/L of biochar)	Vrchovecká et al., 2023
	• AFAC; • SSA, 484.1 m^2/g; • Pore volume, 0.47 cm^3/g	• Adsorption • Endothermic and spontaneous process	• Freundlich isotherm • Pseudo-first-order kinetics	98% at 50 ºC; 374 mg/g (0.1 g/L of biochar)	Balarak et al., 2021
	• $CoFe_2O_4$/NiO@N-PAC; • SSA, 111.88 m^2/g, • Pore volume, 0.033578 cm^3/g (mesoporous structure)	• Adsorption • Exothermic and spontaneous process	• Freundlich model • Pseudo-second-order	98.5%; 2000 mg/L (0.8 g/L of biochar)	Ameen et al., 2023
	• Fe/N-biochar; • SSA, 290.64 m^2/g, • Pore volume, 0.361 cm^3/g	• Adsorption	Not given	Not given	Xu et al., 2022
	• PZBC800 • SSA, 534.91 m^2/g, • Pore volume, 0.335 cm^3/g • Mesopore volume, 0.158 cm^3/g	• Adsorption	Not given	98.9% (0.1 g/L of biochar)	Wu et al., 2022

	• FMPC	• Adsorption • Endothermic process	• Pseudo-second-order kinetic model	87.8% (0.1 g/L of biochar)	Aziz et al., 2024
Spiramycin (SPC)	• BC700; • SSA, 451.68 m^2/g	• Adsorption • Exothermic process	• Langmuir model; • Pseudo-second-order kinetic model	100% at BC700 dosage of 2.0 g/L; 147.28 mg/g	Gao et al., 2022
Metronidazole (MET)	• PCB-900 ºC; • SSA, 597.97 m^2/g at 900 ºC (vs 64.77-353.97 m^2/g at 500-700 ºC); • Micropore volume, 0.24 cm^3/g at 900 ºC (vs 0.026 cm^3/g at 500 ºC and 0.156 cm^3/g at 700 ºC); • Pore volume in mesopores, 2-50 nm with large pore size (average = 2.36 nm > MET geometry)	• Adsorption • Endothermic and spontaneous process	• Langmuir isotherm; • Pseudo-second-order model	98.57% (1.0 g/L of biochar); 138.94 mg/g	Chebbi et al., 2023
	• PT500 • SSA, 301.88 m^2/g • Pore volume, 0.16 cm^3/g	• Adsorption • Non-spontaneous and exothermic adsorption	• Langmuir model • Pseudo-second-order model	88.8% (4.0 g/L of biochar)	Sun et al., 2018
	• Chemically modified biochar (being prepared by activating eucalyptus sawdust powder at 500 ºC with impregnation ratio of 85% H_3PO_4 to the sawdust at 0.62 for 95 min) • SSA, 882.04 m^2/g (vs 32.80 m^2/g without H_3PO_4 activation); • Pore volume, 0.4316 cm^3/g (vs 0.01829 cm^3/g without H_3PO_4 activation)	• Adsorption • Exothermic and spontaneous process	• Freundlich isotherm model • Pseudo-second-order kinetic model	97.1% (1.0 g/L of biochar)	Wan et al., 2016
	• PTBC • SSA, 189.157 m^2/g;	• Adsorption	• Freundlich	Up to 95.44 mg/g (0.5	Azeez et al., 2024

	• Pore diameter: 2.207 nm	• Exothermic and spontaneous process	isotherm model • Pseudo-second-order kinetic model	g/L of biochar)	
	• PJAC • Mesoporous structure • SSA, 358.47 m^2/g; • Total pore volume, 0.189 cm^3/g	• Adsorption • Endothermic and non-spontaneous process	• Langmuir isotherm model • Pseudo-second-order kinetic model	17.33 mg/g (1 g/L of biochar)	Manjunath and Kumar, 2018
	• HS-AC • SSA, 1650.09 m^2/g; • Total pore volume, 1.093 cm^3/g; • Micropore volume, 0.6277 cm^3/g; • External surface area, 432 m^2/g	• Adsorption • Exothermic and spontaneous process	• Langmuir isotherm model • Pseudo-second-order kinetic model	526 mg/g (almost 100% removal using 1 g/L of biochar)	
	• RH-AC • SSA, 2573.45 m^2/g; • Total pore volume, 1.964 cm^3/g; • Micropore volume, 0.9500 cm^3/g; • External surface area, 712.45 m^2/g	• Adsorption • Exothermic and spontaneous process	• Langmuir isotherm model • Pseudo-second-order kinetic model	588 mg/g (almost 100% removal using 1 g/L of biochar)	Yurtay and M. Kılıç, 2023
	• CS-AC • SSA, 2304.76 m^2/g; • Total pore volume, 1.997 cm^3/g; • Micropore volume, 0.6670 cm^3/g; • External surface area, 983.76 m^2/g	• Adsorption • Exothermic and spontaneous process	• Freundlich model • Pseudo-second-order kinetic model	833 mg/g (almost 100% removal using 1 g/L of biochar)	
	• MAGB; • SSA, 1008.97 m^2/g (>599.95 m^2/g for pristine biochar); • Pore volume, 0.51 (0.42 for GB (unmodified biochar without $FeCl_3$ and $ZnCl_2$) with micropores centred at 1-4 nm and 25-30 nm	• Adsorption • Endothermic adsorption	• Freundlich model • Pseudo-second-order rate model	287 mg/g (0.4 g/L of biochar)	Feng et al., 2022

• $CoFe_2O_4$@CMC/HZSM-5 • SSA, 235.21 m^2/g; • Total pore volume, 0.207 cm^3/g; • Pore size, 3.52 nm	• Adsorption • Endothermic and spontaneous process	• Freundlich model • Pseudo-second-order kinetic model	94% (2 g/L of biochar)	Nasiri et al., 2022
• Ni-MMC	• Adsorption • Exothermic and spontaneous process	• Langmuir isotherm model • Pseudo-second-order kinetic model	93.78% (46.73 mg/g at 0.04 g/L of biochar) within 15 min	Hu et al., 2024
ZnO/PiC0.1	Photodegradation	Not given	97.1% at pH 11 (0.1 g/L of biochar)	Cai et al., 2022b
MnFe-LDO-biochar	Photo-Fenton process with H_2O_2	Not given	~ 98% (0.25 g/L biochar at pH 7)	Azalok et al., 2021
PBC-400CuFe	Photo-Fenton process with H_2O_2	• Pseudo-first-order kinetic model	96.3% (0.4 g/L biochar at pH 3)	Cai et al., 2021
PCoF	Photo-Fenton process with H_2O_2	• Pseudo-first-order kinetic model	99% (0.4 g/L biochar at pH 3)	Cai et al., 2023
SMBC600	Fenton-like degradation	/	Close to 100% at pH = 3 (1 g/L of biochar)	Yi et al., 2019
SMBC300, SMBC400 and SMBC500	Fenton-like degradation	/	92.51% with SMBC400 at pH = 3 (0.3 g/L of biochar)	Yi et al., 2020
MBC	Fenton-like degradation	/	Close to 100% at pH = 3 (0.2 g/L of biochar)	Yi et al., 2021
KMBC	KMBC/persulfate system	/	98.4% (0.5 g/L biochar at pH 6.5)	Luo et al., 2022
MMBC	MMBC/persulfate system	/	95.6% (0.7 g/L biochar)	Luo et al., 2023a

	NMBC	NMBC/persulfate system	/	99.6% (NMBC = 0.8 g/L)	Luo et al., 2023b
	Fe-Ce@N-BC	FeCe@N-BC /peroxymonosulfate system	/	97.5% (0.75 g/L)	Xiao et al., 2022
	$NZVI/Cu^0/BC$-3 • Total pore volume, 0.36 cm^3/g	$NZVI/Cu^0/BC$-3/peroxymonosulfate system	/	100% (pH = 3-9 within 15 min using 0.5 g/L of biochar)	Xu et al., 2024
	$Fe_1:Co_2$-bwc/LBE	Electrochemical oxidation	/	98.7% (electrolyte concentration, 0.05 M; pH, 6.4; current density, 30 mA/cm^2)	Sharan et al., 2023
Clindamycin (CLDM)	• P200 and P400; • C200 and C400 (being prepared by pyrolyzing corn straw powder at 200 ºC and 400 ºC, respectively)	Photodegradation	Not given	56.85% with C400 at pH 8.5	Wang et al., 2023
Enoxacin (ENX)	• PZBC800 • SSA, 534.91 m^2/g, • Pore volume, 0.335 cm^3/g • Mesopore volume, 0.158 cm^3/g	Adsorption	Not given	100% removal	Wu et al., 2022
	• MGPH • SSA, 8.32 m^2/g (vs 0.094 m^2/g for GP) • Average pore size distribution, 12.48 nm; • Pore volume, 0.038 cm^3/g	• Adsorption	• Elovich model	11.7 mg/g (1 g/L of biochar)	Bai et al., 2023
	• MPBC • SSA, 122.12 m^2/g for MPBC; 165.18 m^2/g for PBC • Total pore volume, 0.38 cm^3/g for MPBC; 0.46 cm^3/g for PBC • Micropore volume, 0.015 cm^3/g for MPBC, 0.028 cm^3/g for PBC	• Adsorption • Endothermic and spontaneous process	• Freundlich model • Pseudo-second-order model	35.54–60.31 mg/g (0.5 g/L MPBC)	Zhang et al., 2023

Lorazepam (LRZ)	• AC • SSA, 994 m^2/g; • Micropore volume, 0.19 cm^3/g	Adsorption	Not given	Up to 75%	Jaria et al., 2020
	• RM-NPs • SSA, 83.6 m^2/g; • Mean particle size, 13.84 nm	Adsorption	Not given	80% (1.0 g/L of biochar)	Aydın et al., 2021
Oxazepam (OXZ)	• PBFG4 • SSA, 848.22 m^2/g; • Pore volume, 0.36 cm^3/g	Adsorption	• Pseudo-first-order model • Langmuir and Freundlich isotherm models	0.115 mg/g	Calisto et al., 2015; Calisto et al., 2017

[a]SSA, specific surface area

Table 2. Comparison among key aspects of different types of advanced biochar-based materials for removal of specific antibiotics based on current studies (over last ten years)

Types of biochar	**Pyrolysis temperature (ºC; general value)**	**Specific surface area[a]**	**Application in removal processes[b]**	**General dosage (g/L; general value)**	**Operational pH range**	**Products obtained after removal process**
Modified biochar prepared by pyrolysis	400-950	High SSA (e.g., up to 2754 m^2/g)	• Adsorption	1.0-2.0	✓ Limited pH range, depending on pH_{pzc} of biochar, and pKa, pKa1, and pKa2 of the antibiotics	➢ Specific antibiotics adsorbed on the biochar
Metal-modified biochar	180-800	Low SSA (e.g., up to 1009 m^2/g)	• Adsorption • Degradation in AOP	< 1.0	✓ A wide pH range (e.g., 3-11 in the NZVI/Cu^0/BC-3/PMS system, 3-7 in the $CuFe_2O_4$@BC-assisted photo-Fenton process)	➢ Degraded products, including small molecular products (e.g., NO_3^-/NO_2^-), and/or CO_2 and H_2O

[a]SSA, specific surface area
[b]AOP, advanced oxidation process

Declaration of Competing Interest

The authors declare that they have no known competing financial interests or personal relationships that could have appeared to influence the work reported in this paper.

Highlights

- Properties of modified biochar for removal of specific antibiotics are discussed.
- Removal mechanisms with different modified biochar are reviewed.
- Modified biochar at high pyrolysis temperature favours adsorption of pollutants.
- Metal-modified biochar involves in adsorption and degradation of pollutants.
- Future studies focus on development of novel biochar with excellent properties.

Graphical abstract